Vlasov models for kinetic Weibel-type instabilities

A. Ghizzo, M. Sarrat, D. Del Sarto

Vlasov models for kinetic Weibel-type instabilities

A. Ghizzo[1]†, M. Sarrat[1], D. Del Sarto[1]

Address: 1. Institut Jean Lamour UMR 7198, Université de Lorraine, BP 70239 F-54506 Vandoeuvre les Nancy, France.

† Email address for correspondance: alain.ghizzo@univ-lorraine.fr

Abstract

The Weibel instability, driven by a temperature anisotropy, is investigated within different kinetic descriptions based on the semi-Lagrangian full kinetic and relativistic Vlasov-Maxwell model, on the multi-stream approach, which is based on a Hamiltonian reduction technique, and finally, with the full pressure tensor fluid-type description. Dispersion relations of the Weibel instability are derived using the three different models. A qualitatively different regime is observed in Vlasov numerical experiments depending on the excitation of a longitudinal plasma electric field driven initially by the combined action of the stream symmetry breaking and weak relativistic effects, in contrast with the existing theories of the Weibel instability based on their purely transverse characters. The multistream model offers an alternate way to simulate easily the coupling with the longitudinal electric field and particularly the nonlinear regime of saturation, making numerical experiments more tractable, when only a few moments of the distribution are considered. Thus a numerical comparison between the reduced Hamiltonian model (the multi-stream model) and full kinetic (relativistic) Vlasov simulations has been investigated in that regime. Although nonlinear simulations of the fluid model , including the dynamics of the pressure tensor, have not been carried out here, the model is strongly relevant even in the three dimensional case.

1 Introduction

The Weibel instability (WI) is one of the most basic and long-studied collective plasma processes. This instability, which is a purely growing non-resonant electromagnetic mode ($Re\,(\omega) = 0$), produces strong magnetic fields in plasmas by releasing the free energy stored in the temperature anisotropy. A fraction of the kinetic energy of the plasma is

thus converted into the generation of strong quasi-static magnetic fields through the redistribution of currents in space. This instability was first predicted by Weibel 1959. A simple physical interpretation provided the same year by Fried 1959 showed the equivalence of a strongly anisotropic distribution with a two-stream configuration of a cold plasma. This second kind of instability is usually referred as the current filamentation instability (CFI). In CFI the instability is driven by the momentum anisotropy instead of the temperature anisotropy such as in the WI.

There has been a significant revival in theoretical studies of the WI because it is viewed as highly relevant to at least two areas of science: astrophysics of gamma-ray flares (see Cerruti 2014) and cosmological magnetic field generation (see Schlickeiser et al 2003, Lazar 2009; Medvedev et al 2006; Schoeffller 2016) and the fast ignition scenario for inertial confinement fusion (see Shvets 2009; Silva 2002). In contrast to standard geometry implicated in WI, recent theoretical studies of Bret 2009, 2010; Bret, Gremillet, Dieckman 2010 have also shown the importance of oblique modes.

Relying on the similarity between WI and CFI instabilities, we have recently built a new theoretical tool starting from the possibility of representing the temperature anisotropy by means of a finite number of counter-streaming streams (see Inglebert et al 2012; Ghizzo, Bertrand 2013a and Ghizzo 2013b). This model, we have called the multi-stream model, turns out to be of more general importance and not limited to the Weibel instability.

However the mechanism behind magnetic field generation and the resulting particle trapping, as well as, the life span of these magnetic structures are still unknown issues, which can only be definitively addressed in a kinetic framework. While kinetic effects in wave-particle interactions seem to play a major role in WI, recent theoretical studies, based on fluid approach, as the work of Basu 2002, or the recent work of Sarrat et al 2016a, lead to remarkable results. The resulting macroscopic description, based on the moment equations including the full pressure tensor dynamics, seems to provide a quite complete and accurate picture of WI (a kinetic description of linear Weibel instability being quite cumbersome from an analytical point of view). This somewhat paradoxical result seems to indicate that only a few moments of the distribution function are necessary to give a global picture of the instability. This assumption merits to be validated (or invalidated). Doing so requires to understand the subtle plasma physics of the interactions among particles and the magnetic field. A systematic way to make progress is to test this assumption in the framework of the multi-stream model with direct comparison with full kinetic Vlasov simulations.

If the fluid treatment leading to the derivation of the dispersion relation shows that the pressure tensor $\mathbf{\Pi}$ plays a crucial role in the growth of the instability, one may expect that a small number of streams in the multi-stream description is sufficient to recover the

main features of the instability -the number of streams fixes indeed the number of free parameters which determine the equivalence between the multi-stream and full Vlasov model up to a certain moment of the distribution function f -see Sarrat et al (2016a); Inglebert (2011)-. If this requirement of a small number of streams (or of the "equivalent" moments of f, in a sense which we will discuss next) was to emerge as consistently valid for a large set of numerical and physical parameters, this would strengthen the robustness of the fluid-like description for such type of instability (WI) and justify the use of reduced models for the tested regimes. In this spirit, we have studied the Weibel instability by making numerical comparisons between full kinetic Vlasov-Maxwell simulations and the Hamiltonian reduction technique - the multi-stream model- for a different number of streams. Both models are kinetic in nature and it is then possible to obtain, in both considered descriptions, a picture of the dynamics of trapped particles in phase space, a picture usually not available in the fluid approach. We have then performed an analytical comparison between the fluid model based on a full pressure tensor dynamics and the fluid approximation of the multi-stream model.

The advantage of the fluid formalism, when accounting for a kinetic pressure tensor, obviously lies in its analytical tractability. What we show in this paper is that, whether we consider the kinetic dispersion relation for transverse WI, or the fluid model including the dynamics of the Pressure tensor, both yield to a maximum growth rate that is still 25% too high in comparison of Vlasov- Maxwell numerical experiments. A better agreement with full kinetic Vlasov simulations is finally achieved through the multi-stream model, when the coupling of WI with the longitudinal electrostatic branch is realized. One of the major merits of the multi-stream model is to get a comprehensive understanding of the magnetic field generation and its feedback mechanism on the longitudinal electric field generation. The barrier goes beyond the difficulty to take into account strong relativistic effects to the challenge of bridging these two separate worlds, that are the kinetic and fluid approaches.

The paper is organized as follows. In Section 2 we briefly present the basic equations of the different models. In Section 3 a numerical simulation has been performed using a 2D2V semi-Lagrangian Vlasov-Maxwell solver to study WI. Comparisons with the case of 1D2V situation were also carried out. Comparisons with the multi-stream model are presented in sec. 4 for different sets of initial streams. Finally we draw our conclusions in sec. 5.

2 Basic equations

2.1 The relativistic Vlasov-Maxwell system

The kinetic evolution of the collisionless electron plasma is described by the Vlasov equation, which in a two-dimensional space (with two momenta, i.e. in a 2D2V description) takes the form

$$\frac{\partial F}{\partial t} + \frac{p_x}{m\gamma}\frac{\partial F}{\partial x} + \frac{p_y}{m\gamma}\frac{\partial F}{\partial y} + e\left(E_x + \frac{p_y B_z}{m\gamma}\right)\frac{\partial F}{\partial p_x} + e\left(E_y - \frac{p_x B_z}{m\gamma}\right)\frac{\partial F}{\partial p_y} = 0 \qquad (1)$$

self-consistently coupled to the Maxwell equations, which for the transverse electric (TE) component of the electromagnetic field write as

$$\frac{\partial E_x}{\partial t} = c^2\frac{\partial B_z}{\partial y} - \frac{J_x}{\varepsilon_0} \qquad (2)$$

$$\frac{\partial E_y}{\partial t} = -c^2\frac{\partial B_z}{\partial x} - \frac{J_y}{\varepsilon_0} \qquad (3)$$

$$\frac{\partial B_z}{\partial t} = \frac{\partial E_x}{\partial y} - \frac{\partial E_y}{\partial x} \qquad (4)$$

Here $\gamma = \sqrt{1 + \frac{p_x^2}{m^2c^2} + \frac{p_y^2}{m^2c^2}}$ denotes the Lorentz factor. The electron current density $\boldsymbol{J}$ is given by

$$\boldsymbol{J} = \iint dp_x dp_y \frac{\boldsymbol{p}F}{m\gamma} \qquad (5)$$

In our numerical experiments, we use normalized quantities: time t, space coordinates x, y and momentum coordinates p_x, p_y are respectively normalized to the inverse plasma frequency ω_p^{-1}, the electron skin depth d_e and mc. The electric field components E_x, E_y are normalized to $m\omega_p c/e$ while the magnetic part B_z is normalized to $m\omega_p/e$. We adopt periodic boundary conditions in both x and y directions. Details of the numerical code can be found in Ghizzo 2003 and in the forthcoming paper of Ghizzo (2017) for a hybrid OpenMP- MPI parallelized version of the code.

2.2 The (non-relativistic) Pressure tensor fluid model

We now briefly recall a fluid model for the description of WI based on the inclusion of the full pressure tensor dynamics, which allows a simple interpretation of some physical features of WI, notably the role played by kinetic effects in the non relativistic regime. Recently the linear analysis first performed by Basu 2002 has been extended by Sarrat et

al 2016a and Bret (2006) to include the coupling between WI and CFI and in Sarrat et al (2016b) , the onset of the time-resonant WI has been also studied in this extended fluid model. The fluid set of equations we consider here for electrons in a neutralizing static ion background has been previously considered to study the propagation, when ion pressure anisotropy is allowed, of electromagnetic waves perpendicular to an equilibrium magnetic field (see Del Sarto et al (2015)) and to show how a sheared velocity field may generate long standing non-gyrotropic pressure anisotropy from an initially isotropic configuration (see Del Sarto (2016) for more details). Let us recall the basic equations we need here. By writing the first three moments of the non relativistic Vlasov equation, we have

$$\frac{\partial n}{\partial t} + \boldsymbol{\nabla}.\left(n\boldsymbol{u}\right) = 0 \tag{6}$$

$$\frac{\partial \boldsymbol{u}}{\partial t} + \boldsymbol{u}.\boldsymbol{\nabla}\boldsymbol{u} = \frac{e}{m}\left(\boldsymbol{E} + \boldsymbol{u}\times\boldsymbol{B}\right) - \frac{\boldsymbol{\nabla}.\boldsymbol{\Pi}}{nm} \tag{7}$$

$$\frac{\partial \boldsymbol{\Pi}}{\partial t} + \boldsymbol{\nabla}.\left(\boldsymbol{u}\boldsymbol{\Pi}\right) + \boldsymbol{\nabla}\boldsymbol{u}.\boldsymbol{\Pi} + \left(\boldsymbol{\nabla}\boldsymbol{u}.\boldsymbol{\Pi}\right)^{\boldsymbol{T}} = \frac{e}{m}\left(\boldsymbol{\Pi}\times\boldsymbol{B} + \left(\boldsymbol{\Pi}\times\boldsymbol{B}\right)^{T}\right) - \boldsymbol{\nabla}.\boldsymbol{Q} \tag{8}$$

Here apex "T" denotes the matrix transpose and $\boldsymbol{\Pi} = nm\left(\langle\boldsymbol{v}\boldsymbol{v}\rangle - \boldsymbol{u}\boldsymbol{u}\right)$ is the pressure tensor and $\boldsymbol{Q} = mn\left\langle(\boldsymbol{v}-\boldsymbol{u})(\boldsymbol{v}-\boldsymbol{u})\left(\boldsymbol{v}-\boldsymbol{u}\right)\right\rangle$ is the heat flux tensor where $\langle.\rangle$ denotes an average operation in the velocity coordinate $\boldsymbol{v}$ with respect to the distribution function. A dispersion relation of WI, providing a relatively simpler analytical framework than the kinetic description, can be derived in the linear regime by considering the perturbed quantities of the pressure tensor $\Pi^{(1)}_{xy}$. Linearization of Eqs. (6), (7) and (8) and of the corresponding Maxwell's equations is straightforward. Starting from an homogeneous state characterizing an equilibrium full pressure tensor of the kind:

$$\boldsymbol{\Pi}^{(0)} = \begin{pmatrix} \Pi^{(0)}_{xx} & 0 & 0 \\ 0 & \Pi^{(0)}_{yy} & 0 \\ 0 & 0 & \Pi^{(0)}_{zz} \end{pmatrix} \tag{9}$$

the following set of linearized equations describing the dynamics along y is obtained:

$$u^{(1)}_{y} = \frac{ie}{m\omega}E^{(1)}_{y} + \frac{k}{mn^{(0)}\omega}\Pi^{(1)}_{xy} \tag{10}$$

$$\Pi^{(1)}_{xy} = \frac{k}{\omega}u^{(1)}_{y}\Pi^{(0)}_{xx} + \frac{ie}{m}\frac{\Pi^{(0)}_{yy} - \Pi^{(0)}_{xx}}{\omega}B^{(1)}_{z} \tag{11}$$

$$B^{(1)}_{z} = \frac{k}{\omega}E^{(1)}_{y} \tag{12}$$

$$-ikB_z^{(1)} = e\mu_0 n^{(0)} u_y^{(1)} - \frac{i\omega}{c^2} E_y^{(1)} \tag{13}$$

Superscripts (0) and (1) in Eqs (10) to (13) stand respectively for equilibrium and perturbed quantities and perturbations of type $e^{i(kx-\omega t)}$. Thus the initial configuration is unstable to a pure Weibel mode and the condition $det(\boldsymbol{c^2 D}) = 0$, where $c^2\boldsymbol{D}$ is the standard dispersion matrix, gives two branches. The first one is the classic Bohm-Gross dispersion relation obtained from

$$D_{xx} = \omega^2 - \left(\omega_p^2 + 3k^2 a_x^2\right) = 0 \tag{14}$$

and the second one is linked to the excitation of a transverse electromagnetic mode:

$$D_{zz} = D_{yy} = \omega^2 - k^2 c^2 - \omega_p^2 \frac{\omega^2 + k^2\left(a_y^2 - a_x^2\right)}{\omega^2 - k^2 a_x^2} = 0 \tag{15}$$

Here we have introduced

$$a_x^2 = \frac{\Pi_{xx}^{(0)}}{mn^{(0)}} \qquad \text{and} \qquad a_y^2 = \frac{\Pi_{yy}^{(0)}}{mn^{(0)}} \tag{16}$$

corresponding to thermal velocities. We focus now our attention on condition (15), which can be rewritten in the form of a polynomial of degree four where $\omega_k^2 = \omega_p^2 + k^2 c^2$:

$$\omega^4 - \omega^2\left(\omega_k^2 + k^2 a_x^2\right) + k^2\omega_k^2 a_x^2 - k^2\omega_p^2 a_y^2 = 0 \tag{17}$$

Solving Eq. (17) leads to the WI growth rate,

$$\Gamma_{WI} = \left(\frac{\sqrt{\Delta}}{2} - \frac{\left(\omega_p^2 + k^2\left(a_x^2 + c^2\right)\right)}{2}\right)^{\frac{1}{2}} \tag{18}$$

and the standard cut-off in wave number k_c is recovered in the form:

$$\frac{k_c c}{\omega_p} = \sqrt{\frac{a_y^2}{a_x^2} - 1} \tag{19}$$

where $\Delta = \left(\omega_k^2 - k^2 a_x^2\right)^2 + 4\omega_p^2 k^2 a_y^2 > 0$. A few features, more extensively discussed in Sarrat et al (2016a), shall be pointed out:

(i) The growth rate Γ_{WI} in Eq. (18) was found stronger than the kinetic value obtained from the kinetic relation, which writes as:

$$\omega^2 = k^2 c^2 + \omega_p^2\left(1 + \frac{a_y^2 W(\xi)}{a_x^2}\right) \tag{20}$$

where $W(\xi) = -(1 + \xi Z(\xi))$, $Z(\xi)$ being the plasma dispersion relation of argument

$\xi = \frac{\omega}{\sqrt{2}ka_x}$, and a_x and a_y stand here for the thermal velocities in the x and y directions, in agreement with the notation of Eq. (16). Both dispersion relations (15) and (20) give the same cut-off wave vector.

(ii) A small number of moments is necessary to recover the main features of WI.

(iii) In contrast to the full kinetic treatment, the derivation of the fluid-type dispersion relation shows that the pressure tensor perturbation $\Pi_{xy}^{(1)}$ plays a crucial role in the instability. In Eq. (11) the contribution of the second term related to the anisotropy of the distribution function allows the propagation of low frequency waves.

(iv) The last point concerns the closure condition, we have used here ($\boldsymbol{\nabla}.\boldsymbol{Q} = 0$), which differs from the choice made by Basu 2002 to keep this heat flow but to assume that thermal effects remain weak, leading to the condition that $\varepsilon = \frac{ka_x}{\omega} \ll 1$. In that case, Eq. (15) reduces to

$$D_{yy} = \omega^2 - k^2c^2 - \omega_p^2\left(1 + \frac{k^2a_y^2}{\omega^2}\right) = 0 \tag{21}$$

which corresponds indeed to the condition of hydrodynamic limit of the kinetic dispersion relation of WI (note however than in this hydrodynamical limit the contribution of the heat flux gradient vanishes). The consistent result obtained with the pressure tensor model, while a priori neglecting $\boldsymbol{\nabla}.\boldsymbol{Q}$, agrees with the successful description of the WI by means of only three initial streams in velocity space, as we will see later, at least in the linear regime of WI.

The analysis we have summarized could be in principle adapted to the relativistic regime, in which reasoning in terms of dynamical pressure forces may be easier than in terms of temperatures as far as the anisotropy is concerned. This is however a subject of further studies and for the purposes of the present discussion we will restrict the comparison with the kinetic and multi-stream models to the non-relativistic regime.

2.3 The multistream model

2.3.1 The Hamiltonian reduction technique of the Vlasov equation

Here we restrict our analysis to plane waves propagating along x. The Hamiltonian of a relativistic particle reads as

$$H = mc^2\left(\gamma - 1\right) + e\phi\left(x, t\right) \tag{22}$$

In Eq. (22) ϕ denotes the electrostatic potential. The multi-stream model is a Hamiltonian reduction technique linked to the fact that y does not appear explicitly. Therefore the corresponding Hamilton equation writes as

$$\frac{dP_{cy}}{dt} = -\frac{\partial H}{\partial y} = 0 \tag{23}$$

since the Hamiltonian H is assumed to depend only the longitudinal spatial coordinate x. From (23) it is then possible to reduce the dimension of the global phase space by using the invariance of the generalized canonical momentum (here along y) defined as

$$P_{cy} = p_y + eA_y\left(x,t\right) = const = C_j \tag{24}$$

Here A_y is the y- component of the potential vector. Without loss of generality we can consider a plasma where the particles are divided into $2N+1$ "bunches" of particles (here called "streams"), where each stream noted j (for $|j| \leq N$) constitutes a class of exact solution of the Vlasov equation, having the same initial perpendicular momentum along p_y denoted by the quantity C_j. We can now define, for a population j, a reduced Vlasov-type equation and a corresponding distribution function $f_j\left(x,p_x,t\right)$. The Hamiltonian of one particle of the stream j is then given by $H_j = mc^2\left(\gamma_j - 1\right) + e\phi$, where the new expression of the Lorentz factor, defined for the stream j, is given by:

$$\gamma_j = \sqrt{1 + \frac{p_x^2}{m^2c^2} + \frac{\left(C_j - eA_y\left(x,t\right)^2\right)}{m^2c^2}} \tag{25}$$

and f_j satisfies the reduced Vlasov equation:

$$\frac{\partial f_j}{\partial t} + \frac{p_x}{m\gamma_j}\frac{\partial f_j}{\partial x} + \left(eE_x - \frac{1}{2m\gamma_j}\frac{\partial}{\partial x}\left(C_j - eA_y\right)^2\right)\frac{\partial f_j}{\partial p_x} = 0 \tag{26}$$

Thus for each population j, we now define the stream density as $n_j = \int f_j dp_x$ and the current density

$$J_{y,j} = \frac{e}{m}\left(C_j - eA_y\right)\int_{-\infty}^{+\infty}\frac{f_j}{\gamma_j}dp_x = \frac{e}{m}\left(C_j - eA_y\right)\rho_j\left(x,t\right) \tag{27}$$

Finally the reduced Vlasov-type equations (26) are coupled, in a self-consistent way, to the Poisson equation:

$$\frac{\partial E_x}{\partial x} = \frac{e}{\varepsilon_0}\left(\sum_{j=-N}^{N} n_j\left(x,t\right) - n_0\right) \tag{28}$$

and to the potential vector equation given by

$$\frac{\partial^2 A_y}{\partial t^2} - c^2\frac{\partial^2 A_y}{\partial x^2} = \frac{1}{\varepsilon_0}\sum_{j=-N}^{N} J_{y,j}\left(x,t\right) \tag{29}$$

At this step, two remarks are due:

(i) It is possible to generalize the model to a two-dimensional x, y plasma and to replace the kinetic p_z component of the momentum by its corresponding canonical invariant $P_{cz} = p_z + eA_z(x, y, t) = const = C_j$ (for more details see Begue 1999). Thus the necessary condition for applying the conservation of the transverse canonical momentum is the possibility to separate both electrostatic and electromagnetic contribution in the electric field.

(ii) In the work of Inglebert et al 2012, we have shown that the concept of temperature can be recovered in the perpendicular direction (here p_y) by considering the first moments of the distribution function.

2.3.2 The linear dispersion relation in the multi-stream description

We now focus on the possibility of deriving a generalized dispersion relation for WI in the multi-stream model. By assuming hot streams, initially at equilibrium located on C_j in the momentum coordinate, the reduced distribution function can be linearized in the standard way:

$$f_j(x, p_x, t) = n_0 \alpha_j F_{0j}(p_x) + \delta f_j(k, p_x, \omega) e^{i(kx-\omega t)} \tag{30}$$

In the case of a linear normal mode analysis of the set of Eqs. (26), (28) and (29), in the non relativistic regime, we assume that $A_y = \delta A_y e^{i(kx-\omega t)}$ and $E_x = \delta E_x e^{i(kx-\omega t)}$ where δ denotes a perturbation field. Eqs. (26) gives (using the notation $v_x = \frac{p_x}{m}$):

$$\delta f_j = \frac{e\delta E_x + ik\frac{C_j}{m} e\delta A_y}{i(\omega - kv_x)} n_0 \alpha_j F'_{0j}(p_x) \tag{31}$$

where F'_{0j} denotes the derivative of the initial distribution function $F_{0j}(p_x)$ over p_x. α_j (given by $\frac{n_j}{n_0}$) and C_j verify the normalization condition $\sum_j \alpha_j = 1$ and the total current $\sum_j \frac{\alpha_j C_j}{m} = 0$.

Using (31), and the Poisson's equation (28), the perturbation term δE_x can be expressed as:

$$ik\delta E_x = \frac{e}{\varepsilon_0} \sum_{j=-N}^{+N} \int_{-\infty}^{+\infty} dp_x \frac{e\delta E_x + \frac{ikC_j}{m} e\delta A_y}{i(\omega - kv_x)} n_0 \alpha_j F'_{0j}(p_x) \tag{32}$$

Finally we obtain the relation

$$\delta E_x \left(ik + im\omega_p^2 \sum_{j=-N}^{+N} \alpha_j \int_{-\infty}^{+\infty} dp_x \frac{F'_{0j}(p_x)}{\omega - kv_x} \right)$$

$$-\delta A_y \left(km\omega_p^2 \sum_{j=-N}^{+N} \alpha_j \frac{C_j}{m} \int_{-\infty}^{+\infty} dp_x \frac{F'_{0j}(p_x)}{\omega - kv_x} \right) = 0 \tag{33}$$

By now by linearizing Eq. (29) we obtain

$$i\delta E_x m\omega_p^2 \sum_{j=-N}^{+N} \frac{\alpha_j C_j}{m} \int_{-\infty}^{+\infty} dp_x \frac{F'_{0j}(p_x)}{\omega - kv_x} +$$

$$\delta A_y \left(-\omega^2 + \omega_p^2 + k^2c^2 - km\omega_p^2 \sum_{j=-N}^{+N} \alpha_j \frac{C_j^2}{m^2} \int_{-\infty}^{+\infty} dp_x \frac{F'_{0j}(p_x)}{\omega - kv_x} \right) = 0 \tag{34}$$

Then assuming, for each stream j, a Maxwellian F_{0j} of thermal velocity $a_{x,j}$ (with the usual definition $a_{x,j}^2 = \frac{k_B T_{x,j}}{m}$) Eqs. (33) and (34) lead to the dispersion relation

$$D_{xx} D_{yy} - D_{xy}^2 = 0 \tag{35}$$

where

$$D_{xx} = \omega^2 \left(1 + \frac{\omega_p^2}{k^2} \sum_{j=-N}^{+N} \alpha_j \frac{(1 + \xi_j Z(\xi_j))}{a_{x,j}^2} \right) \tag{36}$$

$$D_{yy} = \omega^2 - \omega_p^2 - k^2c^2 + \omega_p^2 \sum_{j=-N}^{+N} \frac{\alpha_j C_j^2}{m^2} \frac{(1 + \xi_j Z(\xi_j))}{a_{x,j}^2} \tag{37}$$

and finally

$$D_{xy} = D_{yx} = \frac{\omega \omega_p^2}{k} \sum_{j=-N}^{+N} \frac{\alpha_j C_j}{m} \frac{(1 + \xi_j Z(\xi_j))}{a_{x,j}^2} \tag{38}$$

$Z(\xi_j)$ being the usual plasma dispersion function of argument $\xi_j = \frac{\omega}{\sqrt{2} k a_{x,j}}$ and α_j a normalization constant. Since each stream j has its own temperature along x (given by its thermal velocity $a_{x,j}$), the two longitudinal (Eq. (36)) and perpendicular (Eq. (37)) modes are now coupled by Eq. (38). The decoupling is possible when $D_{xy} = 0$, or equivalently, when each stream has the same longitudinal temperature, thus the term $\frac{(1+\xi_j Z(\xi_j))}{a_{x,j}^2}$ becomes independent of j and we recover the usual relation $\sum_{j=-N}^{+N} \frac{\alpha_j C_j}{m} = 0$ indicating that the total current is zero. In that case Eq. (37) leads to the standard dispersion relation of WI given previously by Eq. (20), which now writes (with $\xi = \frac{\omega}{\sqrt{2} k a_x}$) :

$$\omega^2 - \omega_p^2 - k^2c^2 + \omega_p^2 \frac{(1 + \xi Z(\xi))}{a_x^2} \sum_{j=-N}^{+N} \frac{\alpha_j C_j^2}{m^2} = 0 \tag{39}$$

The comparison with Eq. (20) allows us to define a transverse temperature given by Eq. (41). It must be pointed out, that in a previous works (Ghizzo, Bertrand 2013a), a similar result has been obtained by using a Water-Bag description in the longitudinal

description p_x (where several "bags" a_j were used) while keeping the multi-stream approach in p_y. Thus in the limit where relativistic effects are negligible, we recover the dispersion relation for WI, which now reads as

$$\omega^2 - \omega_p^2 - k^2c^2 - \omega_p^2 k^2 \sum_{j=-N}^{+N} \frac{\alpha_j C_j^2}{m^2\left(\omega^2 - k^2 a_j^2\right)} = 0 \tag{40}$$

which corresponds to the expression (15) in the pressure tensor model.

2.3.3 The hydrodynamic limit of the multistream model and comparison with the fluid model

As shown in the previous example of three non-relativistic beams (cf. Sec.2.3.2), the amount of accuracy with which the initial multi-stream model distribution approximates the initial complete model single-particle distribution, depends on the number of beams: this gives the number of parameters whose values are fixed by the comparison with the fluid moments of the full (Vlasov) kinetic description. Generally speaking, as two parameters are available for each beam $\{\alpha_j, C_j\}$ an initial configuration of N beams can be made to match a Vlasov initial distribution by setting an exact equivalence up to their first $2N$ velocity moments (counting as first moment that of order zero in velocity that is the fluid density). We note in this regard that any initially symmetrical distribution centred around a null average velocity implies all the odd-order fluid moments to be initially zero: an important implication is, for example, that if this symmetry is respected by the global initial multi-stream distribution, the odd-order fluid moments of the multi-stream model remain zero for the whole evolution. Thus in (39) we are capable to define a perpendicular temperature by assuming that the thermal velocity is given by

$$\frac{a_y^2}{c^2} = \sum_{j=-N}^{+N} \frac{\alpha_j C_j^2}{m^2 c^2} \tag{41}$$

For this purpose it is necessary to initialise the system with a distribution of the kind

$$F\left(p_x, p_y\right) = n_0 F_0\left(p_x\right) \sum_{j=-N}^{+N} \alpha_j \delta\left(p_y - C_j\right) \tag{42}$$

Let us now restrict to the case of three streams only ($j = -1, 0, 1$). Assuming symmetry $C_{-1} = -C_1$ and $C_0 = 0$, as it is usually used in such an analysis, the normalization constant α_j (for j varying from -1 to 1) can be directly computed by considering the first moments of the distribution function. Thus we have

$$M^{(2)} = n_0 \sum_{j=-1}^{+1} \alpha_j C_j^2 = \iint p_y^2 F\left(p_x, p_y\right) dp_x dp_y = n_0 m^2 a_y^2 \tag{43}$$

$$M^{(4)} = n_0 \sum_{j=-1}^{+1} \alpha_j C_j^4 = \iint p_y^4 F\left(p_x, p_y\right) dp_x dp_y = 3 n_0 m^4 a_y^4 \tag{44}$$

The case of three streams only, symmetrical in p_y, provides a reduced kinetic description which necessitates initially to know the two first (non null) $M^{(2)}$ and $M^{(4)}$ moment components. Indeed the resolution of the system of Eqs. (43) and (44) requires the determination of $\{\alpha_j, C_j\}$ using symmetry. Thus we obtain $\alpha_1 = \alpha_{-1} = \frac{1}{6}$ and $\alpha_0 = \frac{2}{3}$ (with the normalization condition $\sum_{j=-1}^{+1} \alpha_j = 1$) and finally to $C_{-1} = -C_1 = -\sqrt{3} m a_y$. Thus the ratio of Eq. (44) over (43) writes as $\frac{C_1^2}{m^2} = \frac{3\Pi_{yy}^{(0)}}{m n_0}$. The latter condition expresses the equivalence with the fluid pressure description, at least in the non relativistic regime. The ensemble $\{\alpha_j, C_j\}$ depends from the dynamics of the process under description.

The comparison between results obtained from the multi-stream and from the complete Vlasov model can therefore provide information about the role played by the fluid moments neglected in the multi-stream approach in the dynamics of the phenomenon considered. It is therefore of interest to inquire about the comparison between the multi-stream and the full-pressure tensor-based fluid model in describing Weibel-type instabilities. Even if this subject will deserve dedicated studies, we make here some general remarks, by restricting to the non-relativistic regime of the pure WI (the extensibility to the full-pressure tensor description in the non-relativistic regime requiring indeed further work). To this purpose we first recall the hydrodynamic limit of the multi-stream model, as first introduced in Inglebert 2011.

The multi-fluid model can be obtained by taking the moments of the reduced Vlasov equation (26). We can introduce, for each stream j, a density denoted n_j and a mean velocity u_j. In the assumption where relativistic effects are negligible, for each stream j, the continuity equation and the Euler-like equation write

$$\frac{\partial n_j}{\partial t} + \frac{\partial}{\partial x}\left(n_j u_j\right) = 0 \tag{45}$$

$$\frac{\partial u_j}{\partial t} + u_j \frac{\partial u_j}{\partial x} = \frac{e E_x}{m} + \frac{1}{2m^2} \frac{\partial}{\partial x} \left(C_j - e A_y\right)^2 \tag{46}$$

coupled to Eqs. (28) and (29) using $J_{yj} = e n_j u_j$. Thus approximating the system as a finite number of streams or in other words, as a summation over an ensemble of Dirac distributions. Note that this system of equations is closed with no need of a further equation for the second order fluid moment. Its evolution is therefore completely determined by the two equations above. We have then obtained a "fluid" description equivalent to Eqs.

(6) and (7), formally including the information about the pressure tensor but also on the moments of order 4 in velocity (again expressible in terms of n_j and u_j), and of order 3 and 5 (which shall be null in the case of a WI initialised with a Maxwellian distribution in v_x).

2.4 Connection between the multi-stream model and the Pressure tensor dynamics

For completeness, we have investigated the connection between both reduced models, the multi-stream model and the fluid model which takes into account the dynamics of the Pressure tensor. To do that, we retain the concept of "stream" in the framework of a "multi- fluid" approach by introducing, for each stream j, a pressure tensor $\Pi^{(j)}_{\alpha\beta}$. This highlights the importance of a correct (and pedagogical) modeling of the nonlinear interaction between streams, where the possibly relevant ingredients, such as the global pressure tensor are retained. Moreover, the approach presented here can give insights into the coupling between WI and CFI. The challenge is to understand how the coupling between CFI and WI gets started at all, leading to the excitation of the electrostatic field component. Since the physical mechanism of WI and CFI being very similar, the amplification of the longitudinal plasma field has to be found again in the symmetry breaking of streams. In the multi-stream approach, each particle "bunch", of density $n_j\left(x,t\right)$, for a given j, can be indeed represented by $\Pi^{(j)}_{\alpha\beta}$, where α and β denote labels to be taken in $\{x,y\,,\,z\}$. Thus it is possible to write the global Pressure tensor $\Pi_{\alpha\beta}$ in the following form:

$$\frac{\Pi_{\alpha\beta}}{mn}=\sum_{j=-N}^{+N}\frac{\Pi^{(j)}_{\alpha\beta}}{mn_j}-\sum_{j=-N}^{+N}\sum_{k\neq j}\frac{n_jn_k}{n^2}u^{(j)}_{\alpha}u^{(k)}_{\beta} \tag{47}$$

where $u^{(j)}_{\alpha}$ denote the mean density of "stream" j, and $u^{(j)}_{\alpha}=\frac{1}{n_j}\int_{-\infty}^{+\infty}v_\alpha f_j dp_x$ and $v_\alpha=v_\alpha\left(x,p_x,C_j\right)$ is the velocity term which may depend explicitly of C_j, after integration over p_y. Here

$$\frac{\Pi^{(j)}_{\alpha\beta}}{mn_j}=\int_{-\infty}^{+\infty}dp_xv_\alpha v_\beta f_j-\frac{n_j}{n}u^{(j)}_{\alpha}u^{(j)}_{\beta} \tag{48}$$

Let us now consider the example of the coupling of WI and CFI. Indeed WI can be described, in the multi-stream approach, by the set of $2N-1$ particle "bunches" or streams, while only two particle "bunches" are required for CFI, say the streams noted $\pm N$. This example can be reformulated in the Pressure tensor dynamics by choosing two streams of momentum $C_{\pm N}$ having different temperatures in p_x and described by the quantities $\Pi^{(\pm N)}_{\alpha\beta}\left(C_{\pm N}\right)$, while the bulk of the plasma is characterized by a diagonal pressure tensor

of type (9). Thus Eq. (47) reads now

$$\frac{\Pi_{\alpha\beta}}{mn} = \sum_{j=-N+1}^{+N-1} \frac{\Pi_{\alpha\beta}^{(j)}}{mn_j} + \frac{\Pi_{\alpha\beta}^{(N)}}{mn_N} + \frac{\Pi_{\alpha\beta}^{(-N)}}{mn_{-N}} - \sum_{j=-N}^{+N} \sum_{k\neq j} \frac{n_j n_k}{n^2} u_\alpha^{(j)} u_\beta^{(k)} \tag{49}$$

In Eq. (49) the first term describes the behavior of WI, the second and third terms CFI and the last term the nonlinear interaction between streams. Thus, in the linear regime, a little algebra yields (see Ref. Sarrat et al (2016a) for more details) to a dispersion relation of the same type than (35) where

$$D_{xx} = \omega^2 - \omega^2 \sum_{j\in\{-N,+N\}} \frac{\omega_{pe,j}^2}{\omega^2 - 3k^2 a_{x,j}^2} \tag{50}$$

$$D_{yy} = \omega^2 - k^2 c^2 - \sum_{j\in\{-N,+N\}} \omega_{pe,j}^2 \left(\frac{\omega^2 + k^2 \left(a_{y,j}^2 - a_{x,j}^2\right)}{\omega^2 - k^2 a_{x,j}^2} + \frac{k^2 C_j^2}{\omega^2 - 3k^2 a_{x,j}^2} \right) \tag{51}$$

$$D_{xy} = -\omega^2 \sum_{j\in\{-N,+N\}} \frac{kC_j}{\omega} \frac{\omega_{pe,j}^2}{\omega^2 - 3k^2 a_{x,j}^2} \tag{52}$$

where $\omega_{pe,j}^2 = \frac{n_j e^2}{m\varepsilon_0}$ is the squared of the plasma frequency of each stream of CFI. Here the D_{xx} contribution is related to the Bohm- Gross oscillations, inherently electrostatic in nature, which for $D_{xy} \neq 0$, couple to the transverse electromagnetic modes related to D_{yy}. Furthermore it must be pointed out that D_{xy} vanishes only if $a_{x,N}^2 = a_{x,-N}^2$ or equivalently when the two beams constituting CFI have the same temperature (the symmetry in that case being preserved).

3 Physical features of the Weibel instability driven by an initial temperature anisotropy

3.1 2D2V full kinetic semi-Lagrangian Vlasov-Maxwell simulations

We now illustrate the physical mechanism for the thermal anisotropy-driven Weibel instability. We have performed simulations of WI with a 2D2V semi-Lagrangian Vlasov - Maxwell code. We present detailed results in Figs. 1 to 5 for a simulation with a relatively short box of length $L_x = \frac{2\pi}{k_0} \simeq 3.590 c\omega_p^{-1}$ corresponding to a wave vector of $k_0 c/\omega_p = 1.75$ and $L_y = 4\pi c\omega_p^{-1}$ in the perpendicular direction. Motivated by direct numerical comparisons, the case of a linear polarization of the electromagnetic field is only considered here. The phase space sampling for the full 2D2V Vlasov simulation (two dimensions in space

plus two dimensions in momentum) is $N_x N_y N_{p_x} N_{p_y} = 256^2 \times 128^2$ and we choose a time step of $\triangle t\omega_p = 0.005$. The code uses a semi-Lagrangian scheme which is fully parallelized and uses local spline interpolation techniques with 256 processors and 4 threads by processor. Details of the numerical scheme can be found in the forthcoming paper of Ghizzo 2017. The initial condition is a standard bi-Maxwellian distribution with a temperature anisotropy corresponding to $T_x = 1keV$ and $T_y = 50keV$.

The initial condition is given by

$$f\left(x, y, p_x, p_y, t = 0\right) = F_{max}\left(p_x, p_y\right)\left(1 + \sum_{n=0}^{3}\sum_{m=0}^{3} \varepsilon \cos\left(nk_{0x}x\right)\cos\left(mk_{0y}y\right)\right)$$

where F_{max} is the Maxwell-Boltzmann distribution function and $\varepsilon = 10^{-4}$ is a small perturbation.

Here we consider a single mode k_0 and assume that only electrons take part in the dynamics. This assumption is valid since the electrons provide the source of free energy which initially causes the instability. Then the system evolves on the relatively fast electron time scale and ions may be considered as an infinitely massive neutralizing background. Although in general WI can occur within a range of wave number k, the fact to consider a numerical box "short" in the x direction (of length $\frac{2\pi}{k_0}$ with k_0 being the most linearly unstable mode) is not only an excellent opportunity to compare the analytic theory with numerical simulations but may also provide a detailed insight of how a more realistic multi-mode plasma evolves and saturates.

On top panel, in Fig. 1, we have plotted the time evolution of the mean relativistic kinetic energy $\epsilon_{kin} = mc^2 \iint \left(\gamma - 1\right) dp_x dp_y$ (dotted line), the total magnetic energy $\varepsilon_{m,z}$ and their mutual sum $\epsilon_{m,z} + \epsilon_{kin}$, which is very close to the total energy of the system because the electric contribution of the electromagnetic energy $\varepsilon_{e,x} + \varepsilon_{e,y}$ remains negligible. We have introduced the following notation (respectively for the magnetic, and for the x and y components of the electric part):

$$\varepsilon_{m,z} = \frac{1}{L_x L_y}\int_0^{L_x}\int_0^{Ly} \frac{B_z^2}{2\mu_0} dxdy \tag{53}$$

$$\varepsilon_{e,x} = \frac{1}{L_x L_y}\int_0^{L_x}\int_0^{Ly} \frac{\varepsilon_0 E_x^2}{2} dxdy \quad \text{and} \quad \varepsilon_{e,y} = \frac{1}{L_x L_y}\int_0^{L_x}\int_0^{Ly} \frac{\varepsilon_0 E_y^2}{2} dxdy \tag{54}$$

The magnetic field energy saturates at about $t\omega_p \simeq 60$. It can be seen that the growth of the magnetic field energy compensates the decrease of the kinetic energy in roughly the same measure, thus conserving the total energy. On bottom panel, we have represented

the growth rate $\frac{\Gamma}{\omega_p}$ as a function of $\frac{kc}{\omega_p}$ using the fully kinetic dispersion relation using the standard Eq. (20) for purely transverse WI in solid line, while the fluid dispersion relation, taking into account the Pressure tensor dynamics is plotted in dashed line (which corresponds to Eq. (15). Both kinetic and fluid models overestimate the growth rate. A detailed calculation shows indeed that there is a coupling with the electrostatic field component, as indicated by Eq. (35). Thus choosing a short length of the system allows us to excite the most unstable mode on the fundamental mode with an expected growth rate of $\frac{\Gamma_{max}}{\omega_p} \simeq 0.24$ (the other harmonics may also occur since their growth rate are not negligible).

The different energy components, as a function of time, are plotted in Fig. 2 in a logarithmic scale. We observe that the electric field energy $\varepsilon_{e,y}$ also grows, at the same growth rate in comparison to the magnetic energy $\varepsilon_{m,z}$, but its amplitude remains very small when compared to the longitudinal electrostatic part $\varepsilon_{e,x}$. In the one-dimensional case, E_y has a purely electromagnetic contribution, while the nature of the longitudinal E_x counterpart is electrostatic. While both E_y and B_z components of the electromagnetic field exhibit the same linear growth rate close to $\frac{\Gamma_{num}}{\omega_p} \simeq 0.192$, the electrostatic part increases at a growth rate about twice as fast $(dE_y/dt)\, E_y \sim 2\Gamma_{num} \simeq 0.384$ in its linear stage, followed by fast oscillations close to a frequency of $\omega \sim 1.18\omega_p$. However it is interesting to note that the level in amplitude of the electrostatic energy $\varepsilon_{e,x}$, although weak in comparison to the magnetic one, is higher than $\varepsilon_{e,y}$.

In many aspects, the numerical results presented here confirm the key role played by two processes: the magnetic trapping and the electrostatic activity. The magnetic trapping is shown to produce a topologically symmetric structure of the distribution function in the form of a rotating magnetic vortex, on the mode k_0, and located in the region of momentum of small density coupled with an electrostatic structure, on a mode twice of k_0, located on the bulk of the distribution.

Furthermore a critical role in the complex interaction between magnetic trapping structures and plasma is expected to be played by the presence of an electrostatic activity. However without perturbation, the plasma is strictly homogeneous in y and the two-dimensional simulation afforded by the Vlasov- Maxwell code gives the same results than those obtained in a one- dimensional treatment. We have just verified that no oblique mode was excited when a small perturbation in the direction y was introduced, a coupling which is in principle possible for a strong anisotropy in temperature or in the strong relativistic regime of the interaction, but which is not relevant in the considered case here.

In three-dimensional (3D) systems, the multi- stream model cannot be applied (since it is not possible to find a "lacking" variable and then a corresponding canonical invariant). However the fluid approach including the pressure tensor dynamics is still possible,

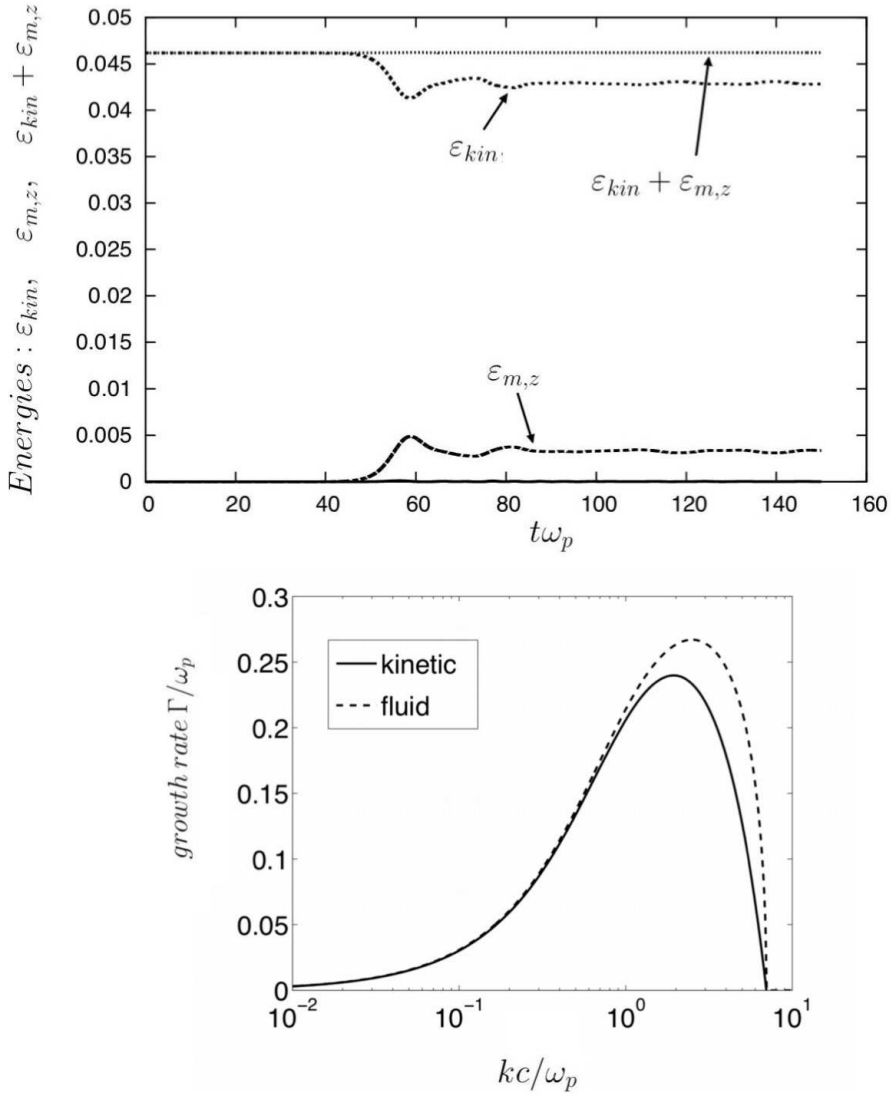

Figure 1: On top panel; the time evolution of the kinetic energy ϵ_{kin}, and of the magnetic energy $\epsilon_{m,z}$ plus their mutual sum $\epsilon_{kin} + \epsilon_{m,z}$, which is conserved at saturation. On bottom panel, the growth rate Γ/ω_p as a function of kc/ω_p for purely transverse WI, using the kinetic treatment (in solid line) or the fluid approach including the pressure tensor dynamics (in dashed line). For transverse WI, the multi stream model gives exactly the same result than the kinetic treatment, while Vlasov numerical experiment gives a somewhat smaller values

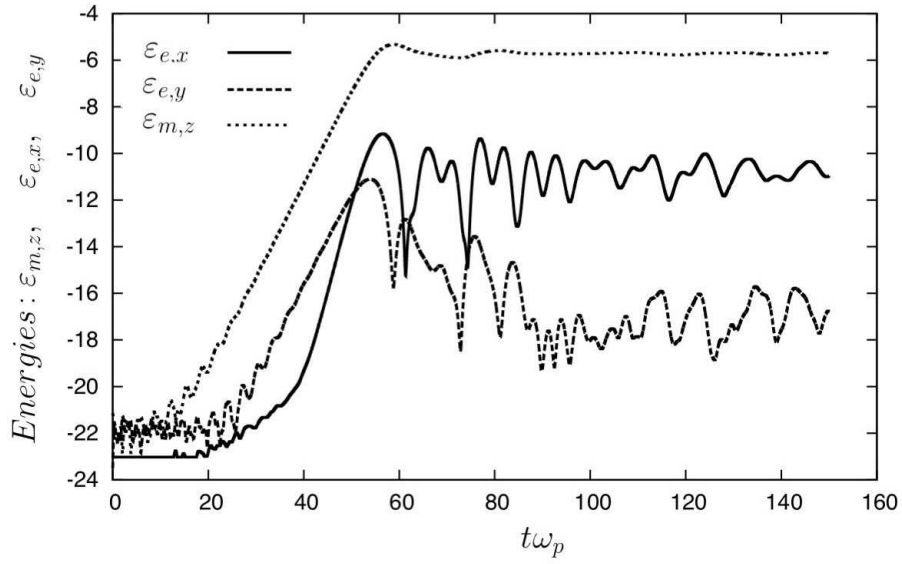

Figure 2: Time evolution, on a logarithmic scale, of the magnetic energy $\epsilon_{m,z}$, of the electrostatic part $\epsilon_{e,x}$ and the electric contribution $\epsilon_{e,y}$ of the electromagnetic energy. We observe that $\epsilon_{m,z}$ and $\epsilon_{e,y}$ grow at the same rate but $\epsilon_{e,y}$ breaks down at saturation indicating that $\epsilon_{m,z}$ has a magnetostatic nature. The growth rate of the electrostatic part $\epsilon_{e,x}$ is twice. Results obtained from the 2D2V Vlasov solver.

showing that such an analysis is particularly relevant in 3D systems, provided that the closure condition is known. The multi- stream model can play a major role in this case, even in a reduced geometry, to test the valididy of the closure condition.

Let us consider now a population of magnetically trapped particles, located at a specific value of p_y. Although they are a minority in number, these trapped particles of the "stream p_y" contribute significantly to the saturation process. They experience a bounce motion with a frequency given by

$$\frac{\omega_b}{\omega_p} = \sqrt{\frac{k_0 c}{\omega_p} \frac{p_y}{mc} \frac{eB_{z,max}}{m\omega_p}} \tag{55}$$

However the situation is somewhat different in the bulk of the distribution since $p_y \sim 0$ and thus the magnetic bounce frequency tends to zero in Eq. (55). As a consequence, there is a change in the nature of the electron dynamics in the bulk of the plasma. Now the longitudinal electric field can be driven non linearly by charge effects (the plasma exhibiting inhomogeneous trapping structures) and it is the self-consistent field that can accelerate individual particles, as can be seen in Fig. 3 at time $t\omega_p = 75$. Note the presence of the dominant mode $2k_0$ at the saturation time $t\omega_p \simeq 56.25$.

Secondly, as revealed by global 1D2V Vlasov simulation in Ghizzo (2013c) (see Fig. 1) and in the papers of Palodhi 2010, 2009, the isolated "streams" can be formed in an

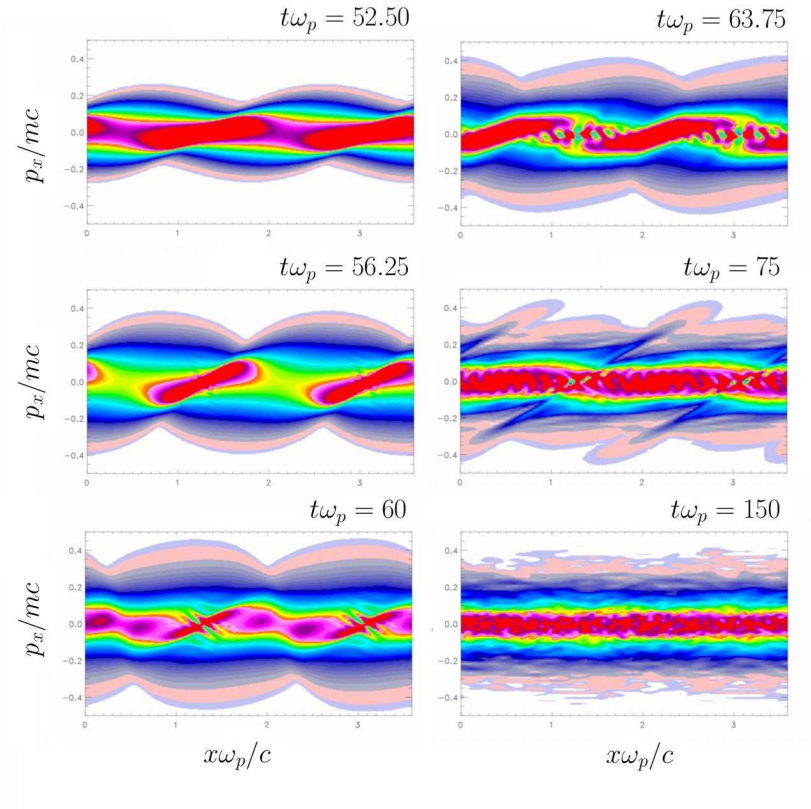

Figure 3: Phase space representation in the $x - p_x$ plane. Results of a simulation performed by the 2D2V SL Vlasov solver. The plots have been obtained by integrating the distribution over the p_y and y variables.

asymmetric way in space, but result located respectively in positive and negative values of p_y. This results in the well-known Y- shape of the distribution in the $x - p_y$ phase space. An example of such behaviour is reproduced in Fig. 4 using the 2D2V Vlasov simulation. The numerical results of the non linear Vlasov simulation not only show that the saturation is governed by strong magnetic trapping, as expected, but evidence that the concept of "stream" is important in WI. As already indicated in Lemons (1979), Innocenti et al (2011) and Inglebert et al (2012), these particle streams are connected to the property of invariance of the canonical momentum in the perpendicular direction and allow to provide a physical picture of WI.

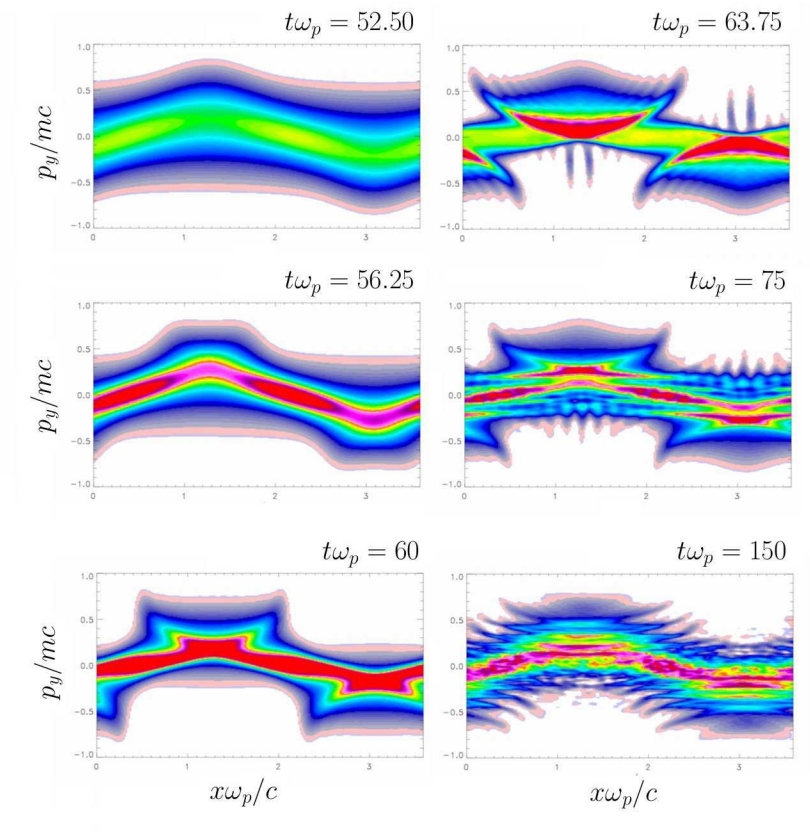

Figure 4: Phase space representation in the $x - p_y$ plane. Results obtained from a simulation performed by the 2D2V SL Vlasov solver. The plots have been obtained by integrating the distribution over the p_x and y variables.

A question remaining to be answered is the role played by the electrostatic fluctuations at the saturation of WI. It is not yet clear whether the "isolated stream" observed for large values of p_y is stable or whether several streams are excited (see the asymptotic state in Fig. 4 at time $t\omega_p = 150$). At the moment the electrostatic field energy is thought to occur in the self- reorganisation of the magnetic field in term of an inverse-type cascade process or in the occurring of a secondary instability, such as the two-stream process invoked by Innocenti et al (2011); Kaang et al (2009). The latter however is a scenario we

cannot take into account here since a single mode dominates throughout the simulation. However the observed fluctuations of the electrostatic field can provide the necessary seed for the growth of the secondary instabilities.

3.2 Comparison with 1D2V full kinetic Vlasov-Maxwell simulations

The assumption of translation invariance along y (y being a lacking variable) is necessary to build the multi-stream model since it is a reformulation of the invariance property of the canonical momentum in the y direction. We observe in Fig. 5, where we have plotted the electron density in space, that perturbations in y maintain a very weak amplitude, indicating that the plasma behaves almost as a one-dimensional system. Thus we can explore this regime of WI directly by using a 1D2V version of the code.

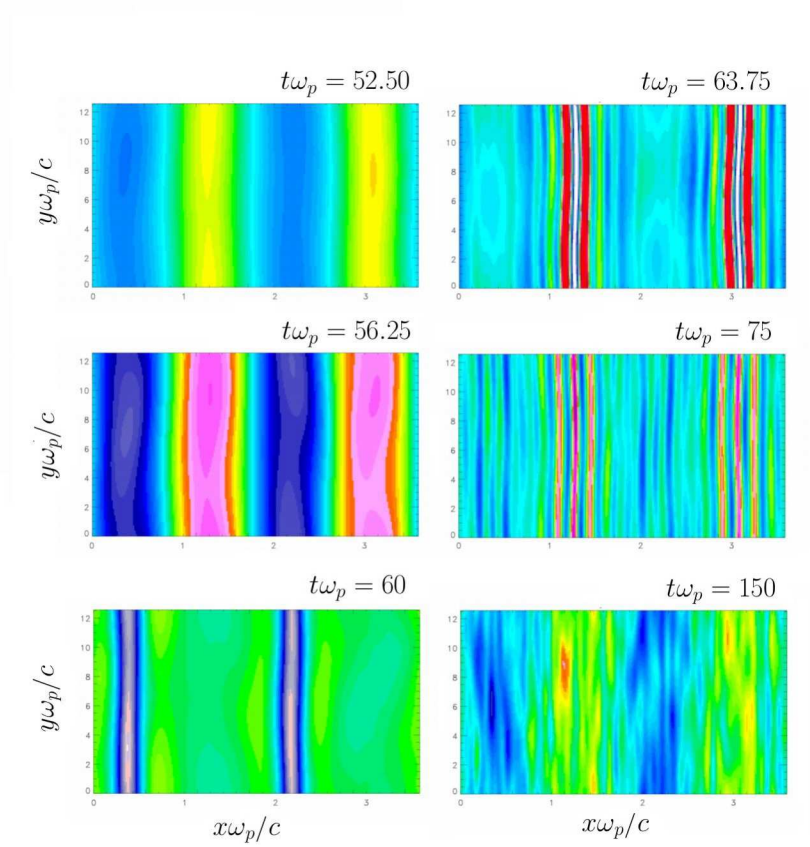

Figure 5: Electron density representation in the $x-y$ plane, obtained from the 2D2V SL Vlasov solver. Electron density fluctuations remain weak in y indicating that the plasma behaves as a one-dimensional system.

We performed a second simulation using now the 1D2V version of the code with the same physical (and numerical) parameters as those used in the 2D2V case, except this

time we chose to increase the resolution in the momentum space up to $N_{p_x} N_{p_y} = 257^2$. Numerical comparison is shown in Figs. 6 and 7. While Fig. 6 shows the time evolution of the magnetic energy $\varepsilon_{m,z}$ for the 2D2V numerical experiment (on thick line) and the 1D2V case (on thin line) superimposed on the same plot. The electrostatic component $\epsilon_{e,x}$ of the electric energy is shown in Fig. 7 (again the corresponding results obtained from the 2D2V and 1D2D versions are shown respectively on thick and thin lines). Compared to the 2D case, the magnetic and (longitudinal) electric components energies exhibit an identical behaviour though with a small shift in time. It must be pointed out that the oscillating behaviour of both energies, after the saturation of WI, is clearly recovered by both models. Indeed we may estimate the magnetic bounce frequency ω_b to be close to $\omega_b \simeq 0.284\omega_p$ by considering the first two successive peaks in the temporal evolution of the magnetic energy. From the analytic expression (55), choosing $k_0 c/\omega_p = 1.75$, $eB_{z,max}/m\omega_p \simeq 0.12$, a typical value of the maximum of the magnetic field after saturation, we obtain, for the perpendicular momentum of the stream of trapped particles, $p_y \sim 0.284^2/(1.75 \times 0.12) \sim 0.38mc$, which is close to the thermal momentum $ma_y = 0.312mc$

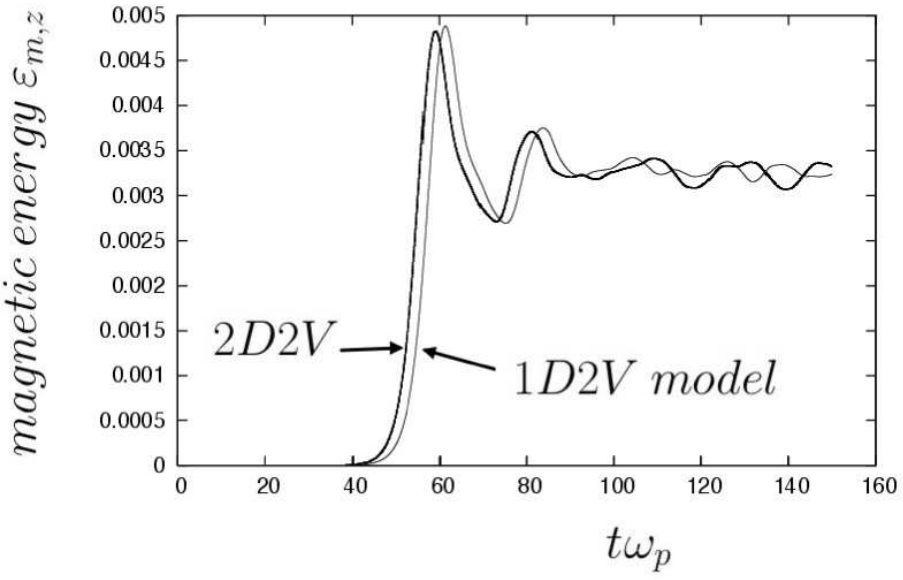

Figure 6: Time evolution of the magnetic energy $\epsilon_{m,z}$, along the z direction, obtained from the 2D2V Vlasov solver on thick line. The result obtained from a 1D2V simulation, shown in thin line, has been superimposed on the plot; showing the same temporal behaviour.

The help of the high resolution phase space diagnostics and the high accuracy afforded by the semi-Lagrangian solver, allow us to give a physical picture of the saturation of WI. To illustrate the process, Figs. 8, 9 and 10 show the representation of the distribution function of $\widetilde{f}(x, p_x)$, $\widetilde{f}(x, p_y)$ and the corresponding distribution of the "beam" located at $p_y = 2ma_y$. Here $\widetilde{f}(x, p_x)$and $\widetilde{f}(x, p_y)$ have been averaged over p_y and p_x respectively.

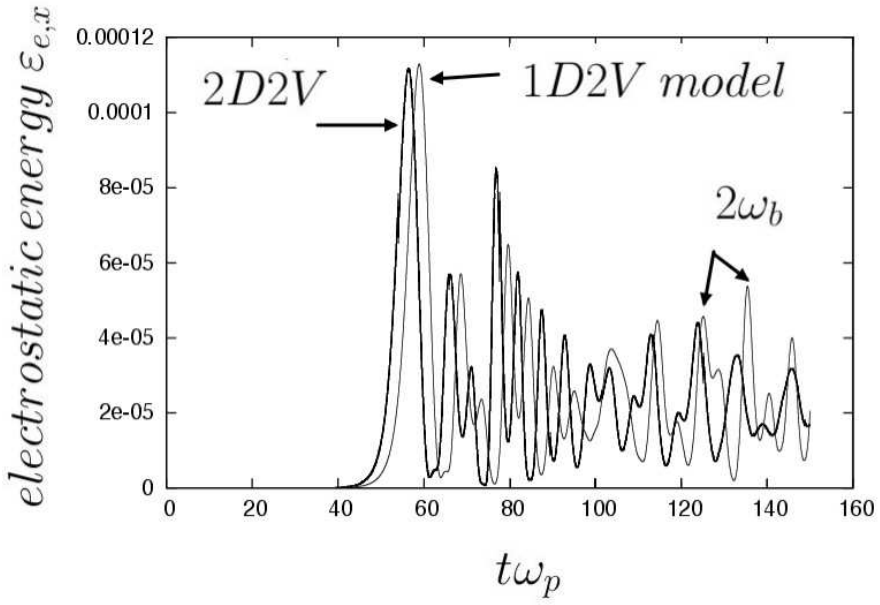

Figure 7: Continuing results of Fig. 6, the time evolution of the electrostatic energy $\epsilon_{e,x}$ obtained from both models: 2D2V on thick line and 1D2V on thin line, superimposed on the plot, showing that fast oscillations are recovered.

The time evolution of these quantities corresponds to half of the magnetic bounce period $\tau_b\omega_p \simeq 11.20$. As first discussed in Palodhi (2010), the electrostatic mode is excited by the deformation of the distribution function due to the differential rotation (rotation depending on p_y) of magnetically trapped electrons in phase space as can be seen in Fig. 10.

The growth of the magnetic field B_z is first accompanied by the growth of E_x. However when B_z reaches its maximum (represented by arrows in Figs. 8 and 9), the electrostatic field breaks down. Furthermore the oscillating behaviour of $\varepsilon_{e,x}$ is characterized, after saturation, by the beating of two frequencies $2\omega_b$ (twice of ω_b since we consider the electrostatic energy) with its harmonics $4\omega_b$, as indicated on top panel in Fig. 7.

Figs. 8 and 9 show the dynamics of the plasma during the first magnetic bounce period. While the top panel, at time $t\omega_p = 60$ in Fig. 8 corresponds to the maximum of $\varepsilon_{e,x}$, the middle panel, at time $t\omega_p = 63.75$, is plotted when $\varepsilon_{e,x}$ tends to zero. Finally the bottom panel in Fig. 8 corresponds to the occurring of the second peak in the plot of the electrostatic energy. One point is especially significant here. The magnetic trapping structure exhibits a dominant mode k_0. Particles are steadily accelerated due to the rotation and the resulting rotating arms, observed in the stream of trapped particles at $p_y = 2ma_y$ in Fig. 10, give rise to the advection motion of plasma observed in Fig. 9. While the distribution in $x - p_x$ (top panel) exhibits an asymmetry near the region of

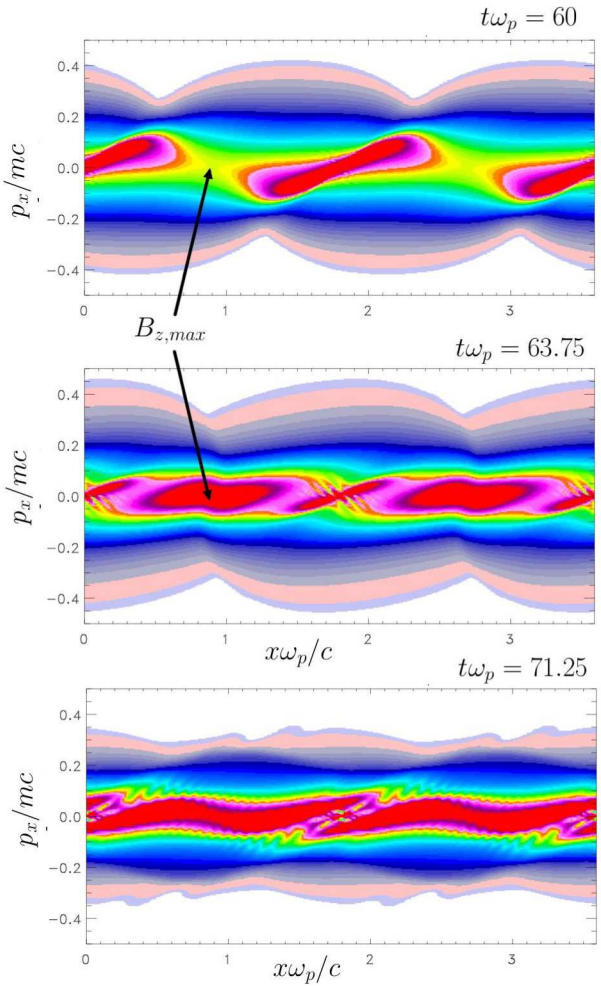

Figure 8: Phase space representation of the averaged distribution function $\widetilde{f}\,(x, p_x)$ afforded by the Vlasov solver in its 1D2V version. The region of high intensity of the magnetic field are indicated by arrows.

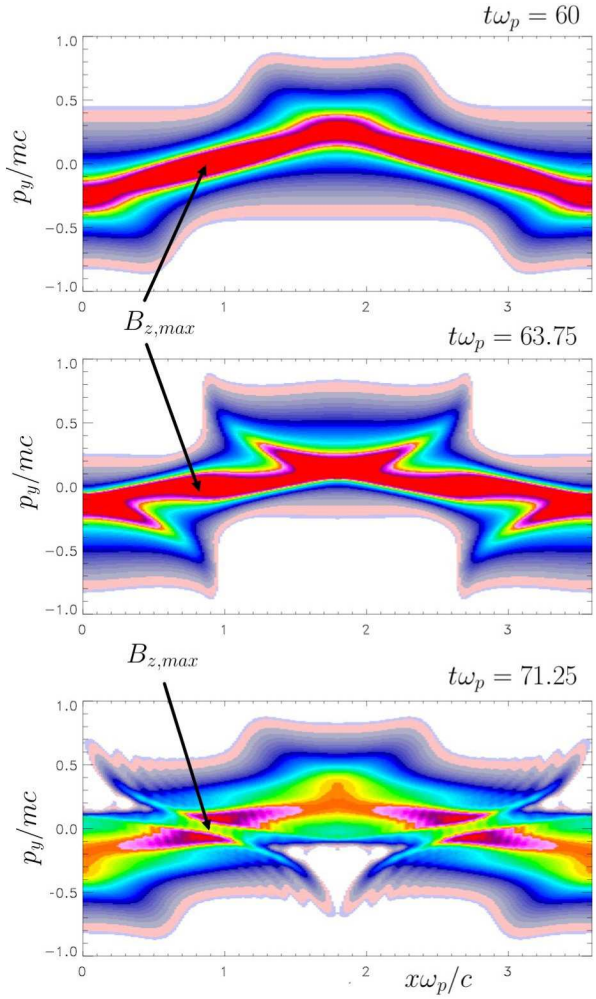

Figure 9: Corresponding representation of the distribution function in the $x - p_y$ plane, the function being integrated over p_x. Results are obtained from the 1D2V version of the Vlasov-Maxwell solver. The distribution exhibits the well-known $Y-$ shape linked to magnetic trapping.

high magnetic field, such asymmetry has disappeared at time $t\omega_p = 63.8$, leading to the formation of a "bump" in the distribution. During this cycle, when the magnetic field energy grows again at time $t\omega_p = 75$, the electrostatic energy increases also and a particle acceleration takes place in region where B_z tends to zero, as can be seen in Fig. 11 , where thin filaments of fast electrons are formed.

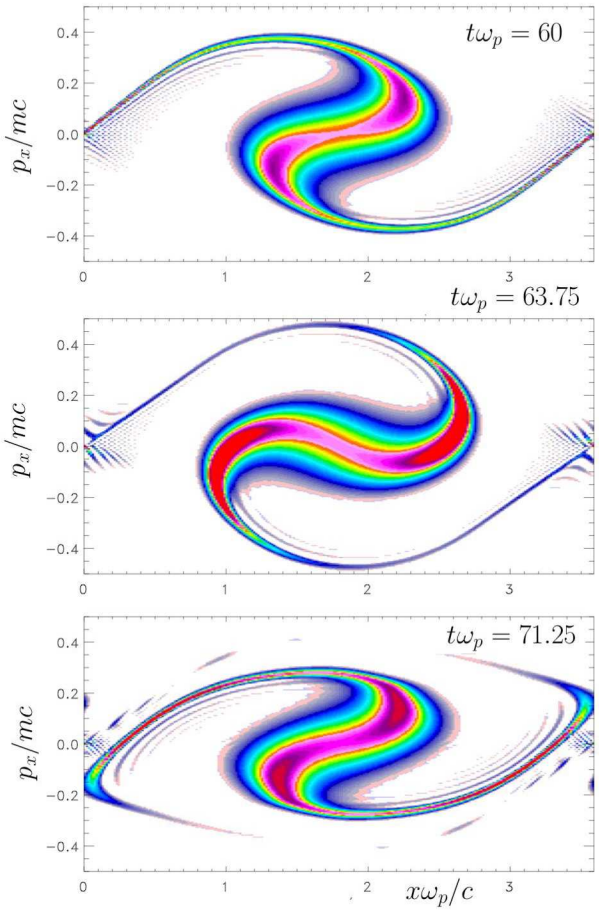

Figure 10: Phase space plots of the 3D distribution function located in the queue of the distribution in p_y at $p_y \simeq 2ma_y$, a_y being the thermal velocity. We observe the formation of a vortex driven by the magnetic trapping.

4 Simulations based on the multi-stream model

To further investigate the central role played by "particle streams" observed in full kinetic Vlasov simulations, we now focus on numerical experiments afforded with the reduced multi-stream code. The use of the canonical invariants allows us to find out a broad class of exact solutions of the Vlasov-Maxwell system. In the full kinetic description, introduced in previous sections, an accurate description of streams of high velocity (and

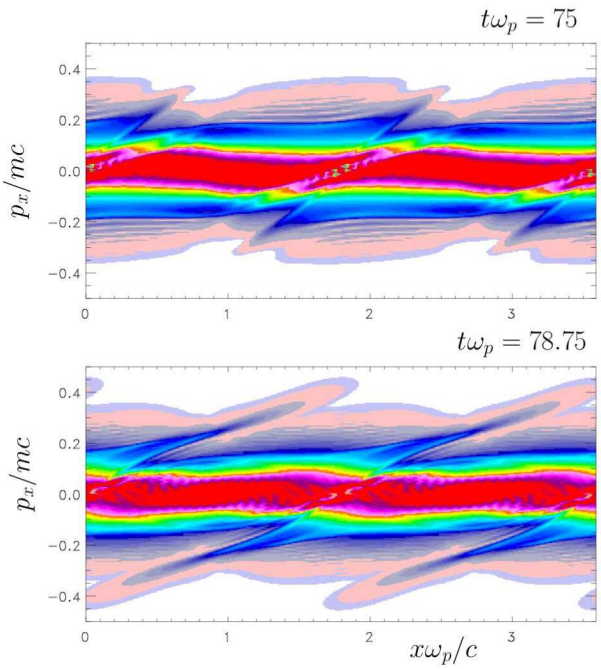

Figure 11: Continuing the plot of $\widetilde{f}\,(x, p_x)$ showed in Fig. 8 when the particle acceleration takes place leading to the formation of thin filaments. Results obtained from the 1D2V Vlasov solver.

therefore of very low densities) becomes difficult from a numerical point of view. In the 1D2V Vlasov code, although noise and accuracy are not severe limits, the resolution in momentum in the p_y direction, required for an accurate description of streams of very weak densities can impose a severe computation burden from a computational point of view. The situation is probably worsened in PIC codes, due to their inherent numerical noise. An alternative is then to consider the multi-stream approach. To show the possibilities of this reduced kinetic model, we choose to start with the case of only three streams (or equivalently with $N = 1$). Numerical simulations using the multi-stream code have been performed using $k_0 c/\omega_p = 1.75$ and the same temperature anisotropy of $T_x = 1keV$ and $T_y = 50keV$. We have used here a phase space sampling of $N_x N_{p_x} = 257 \times 513$. We have also introduced a small perturbation in the magnetic field in the form $\delta B_z = B_0 sink_0 x$. The initial condition, for the distribution function, corresponds here to

$$F\,(x, p_x, p_y, t = 0) = \sum_{j=-1}^{+1} \alpha_j F_{Max}(p_x)\delta\,(p_y - C_j)\,(1 + \epsilon cos(2k_0 x)) \tag{56}$$

Here $F_{Max}\,(p_x)$ is the standard Maxwellian distribution in p_x. The amplitudes of perturbation are $\frac{eB_0}{m\omega_p} = 10^{-5}$ and $\epsilon = 10^{-4}$. Together with the central stream located at $C_0 = 0$ and of density $\alpha_0 = \frac{2}{3}$, we have introduced two other streams at $C_1 = \sqrt{3}mc$ and

$C_{-1} = -C_1$ (with equal densities of $\alpha_1 = \alpha_{-1} = \frac{1}{6}$) using the strict equivalence of the models in the sense of moments (see Eqs (43) and (44) in sec. 2).

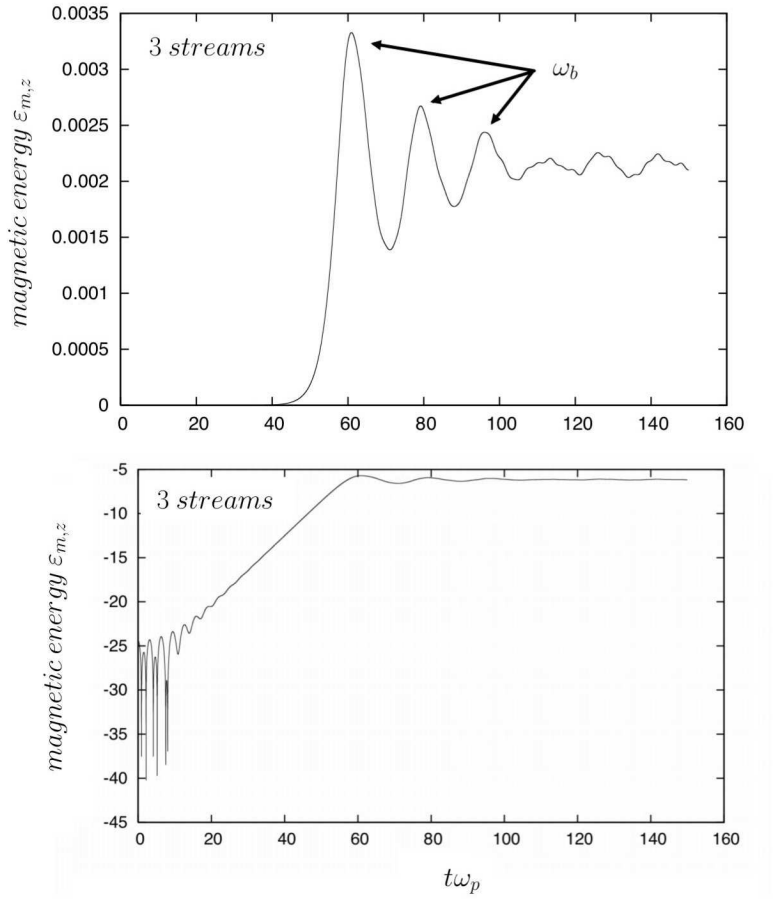

Figure 12: The magnetic energy $\epsilon_{m,z}$ versus time on top panel, using the multi-stream model with only three streams. Bottom panel: the same data in a logarithmic scale versus time, exhibiting an exponential growth in the linear step before saturation.

Fig. 12 exhibits the corresponding time evolution of the magnetic energy on top panel. On bottom panel, in Fig. 12, we have plotted the same quantity in a logarithmic scale.

Due to the exact treatment of invariants and the noiseless character of the semi-Lagrangian approach, our multi-stream model can give important insights on the understanding of kinetic processes arising in the full kinetic Vlasov simulations. In the initial stage of the Weibel instability, the kinetic energy is transferred to the magnetic field. The coupling with the longitudinal electric field is here induced at the beginning of the interaction by weak relativistic effects and the resulting asymmetry in the transverse momentum direction. However part of the energy stored in the electromagnetic field is also transferred back to the stream particles leading to a strong heating of the population of trapped particles, which increases the asymmetry. Thus the bunch of particles (of a given stream) become trapped by the combined action of a weak electric potential and

the magnetic field. The magnetic bounce frequency is clearly present in Fig. 12 (or in Fig. 16 later). Because several bunches of such magnetically trapped particles can involve phase mixing, the bounce frequency is less pronounced in Fig. 6 than in Fig. 12.

As expected, we observe the expected linear phase for $0 \leq t\omega_p \leq 60$) in which the magnetic field energy grows exponentially in time with a numerical growth rate of $\frac{2\Gamma_{num}}{\omega_p} \simeq 0.39$ (the corresponding growth rate of the magnetic being half this value i.e. $\frac{\Gamma_{num}}{\omega_p} \simeq 0.195$), followed by the non linear saturation stage with the characteristic oscillation in time at the magnetic bounce frequency $\omega_b \simeq 0.38\omega_p$ plus a weak damping of oscillations till saturation. The linear phase of WI can be recovered using only three streams, a remarkable result, although the numerical value of ω_b is found somewhat too high in comparison to the expected value obtained in Ghizzo 2013b (part II) reproduced below (in the non relativistic case):

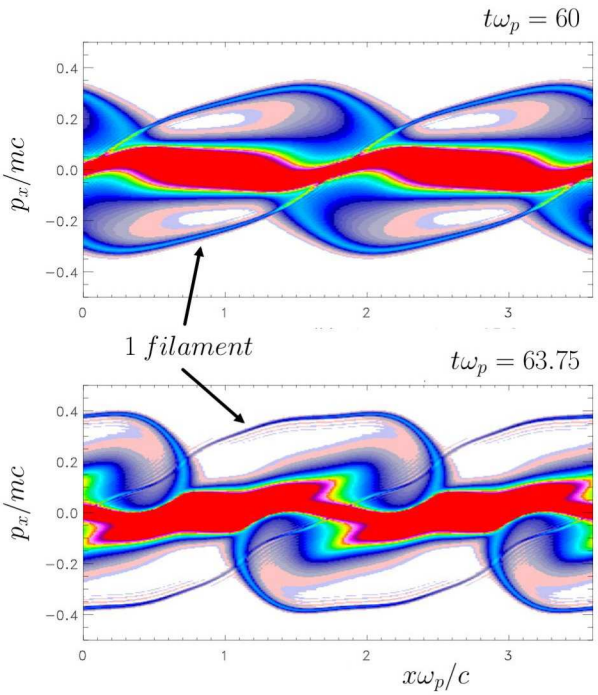

Figure 13: The $x-p_x$ representation of the global distribution built from the three different streams described by the distributions f_{-1}, f_1 and f_0. We see clearly the formation of thin filaments linked to the particle acceleration process for particles of distributions $f_{\pm 1}(x, p_x, t)$.

$$\frac{\overline{\omega}_b}{\omega_p} = \sqrt{\frac{k_0 c}{\omega_p} \sum_{j=-1}^{+1} \frac{\alpha_j C_j}{mc} \frac{eB_{z,max}}{m\omega_p}} \tag{57}$$

Using $\frac{k_0 c}{\omega_p} = 1.75$, the different previous parameters of the streams and a maximum value of the magnetic field of $\frac{eB_{z,max}}{m\omega_p} \simeq 0.12$ (a typical value observed in simulation), we obtain

using Eq. (57) an estimation of $\overline{\omega}_b \simeq 0.348\omega_p$ for the mean bounce frequency. In Fig. 13 we show the global distribution function $\sum_{j=-1}^{+1} f_j$ in phase space at two different times of during the beginning of the saturation. We see clearly the formation of thin filaments of accelerated electrons, a process similar to that observed in Fig. 11.

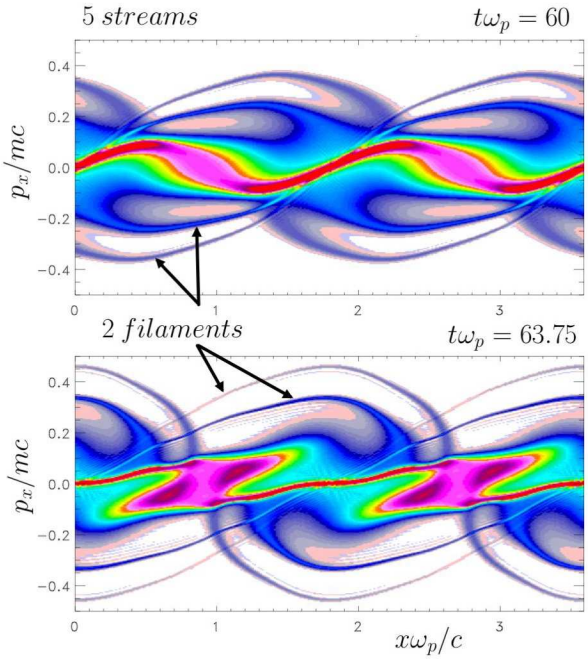

Figure 14: $x - p_x$ phase space for the global distribution function $\sum_{j=-2}^{+2} f_j\,(x, p_x, t)$, at two different times, obtained from the multi-stream model using now five streams located on $C_j = jma_y$. We see the occurring of two filaments for $p_x \geq 0$, each filament being associated to a given stream.

To explore the physics of the multi-stream model, we increase now the number streams to five (i.e. $N = 2$). The physical parameters of streams are $C_j = jma_y$, for $|j| \leq 2$; $\alpha_0 = \frac{1}{2}$,$\alpha_1 = \alpha_{-1} = \frac{1}{6}$ and $\alpha_2 = \alpha_{-2} = \frac{1}{12}$. Fig. 14 shows the corresponding results, equivalent to those of Fig. 13. We see now the occurring of two different processes of acceleration leading to the formation of de-coupled filaments, which get thinner as time goes on. Details of the central region are also shown here. In the non linear phase, each stream with a large value of p_x is subject to the same acceleration mechanism. This scenario is confirmed by Fig. 15 where we have plotted the mean distribution $\overline{F}\,(p_x) = \int \frac{dx}{L_x} \sum_{j=-2}^{+2} f_j\,(x, p_x, t)$ at two different times $t\omega_p = 30$ and $t\omega_p = 60$, which exhibits clearly the two different populations of high energies in the global heating process of WI in the longitudinal p_x direction.

Fig. 16 shows the corresponding time evolution of the magnetic energy $\varepsilon_{m,z}$ obtained in the case of five streams. While the magnetic energy increases exponentially with the same growth rate $\Gamma_{num}/\omega_p \simeq 0.4$, its amplitude reaches a value smaller in comparison with

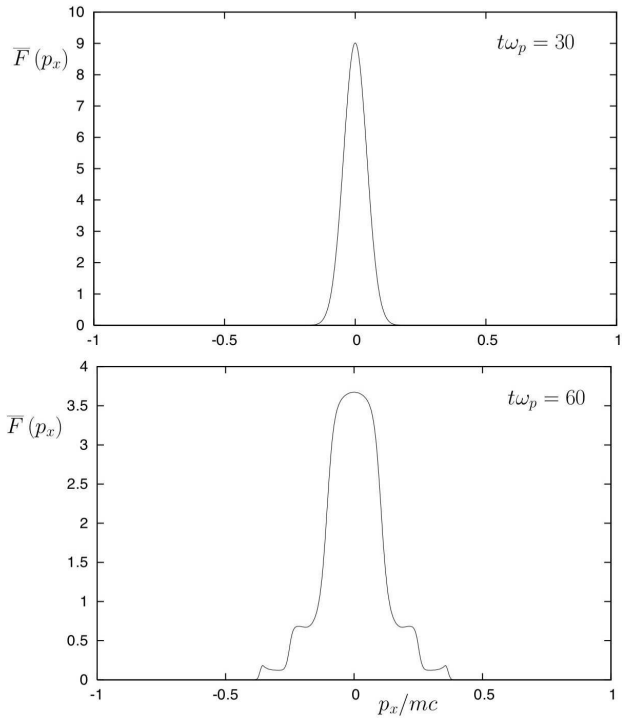

Figure 15: The corresponding plot of the mean distribution $\overline{F}(p_x)$ integrated data of $\sum_j f_j(x, p_x, t)$ over the x variable, at two times, showing that each stream is associated to a (local) longitudinal "heating" process. The results have been obtained from the multi-stream model with five streams ($2N + 1 = 5$).

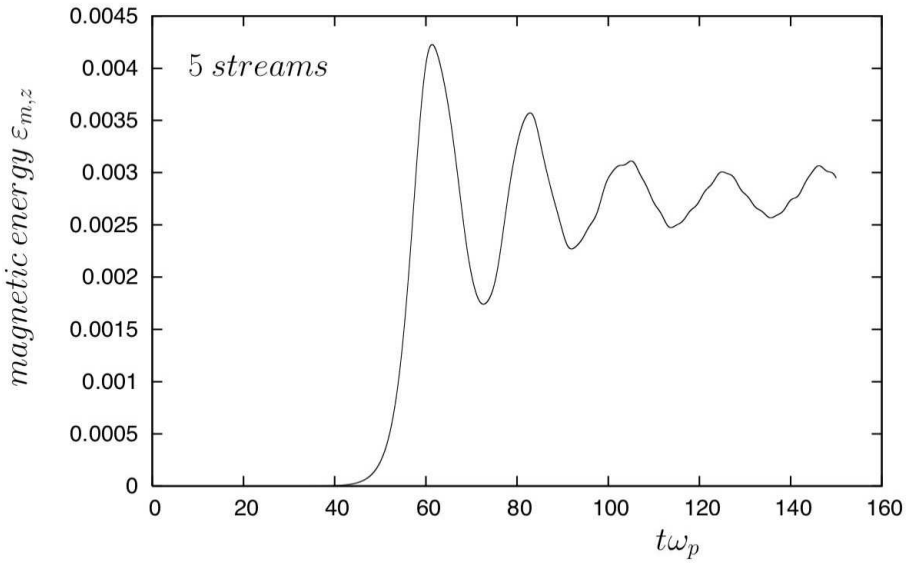

Figure 16: Magnetic energy $\epsilon_{m,z}$ versus time obtained from the multi-stream model in the case of five streams ($2N + 1 = 5$).

the full kinetic code. After saturation, the energy oscillates for a few cycles, decreases in amplitude and the numerical bounce frequencies is close to $\omega_b \simeq 0.28\omega_p$, while Eq. (57) gives $\overline{\omega}_b = 0.21\omega_p$.

Thanks to the possibility to separate the dynamics of the two streams, the model provides the opportunity of more accurate picture of the instability with respect to the full kinetic modelling. The last example we present are the results obtained with a simulation performed with $2N + 1 = 7$ (seven streams). In Fig. 17 we focus on the streams' distribution located at $C_j = 2ma_y$ obtained in both codes, at the same time of $t\omega_p = 67.5$. While on top panel the distribution of trapped electrons has been obtained in the case of the 1D2V Vlasov code, middle and bottom panels correspond to the case of the multi-stream model using $2N+1 = 5$ and $2N+1 = 7$ respectively. We observe the formation of the rotating trapping structure in the $x - p_x$ phase space and the appearance of "arms". The results obtained with the multi-stream model for $2N + 1 = 5$ and with $2N + 1 = 7$ are very similar. Fig. 17 shows that the dynamics is correctly described by the reduced model where only a small number of symmetrical streams is considered. Although the number of streams is restricted, these streams are however described with a high level of accuracy allowing to recover the dynamics of trapped particles. By selecting appropriate initial particle "stream", depending on the problem of interest, the phase space trapping vortices can be thus isolated and examined in detail. Fig. 18 shows the dynamics of the last stream located at $C_3 = 3ma_y$, obtained from the multi-stream model using now seven streams (the streams being initially put on values $C_j = jma_y$ with densities α_j determined with a Maxwellian weight.

The idea to highlight such magnetic trapping structures was already be considered by Innocenti et al (2011) using PIC simulations. In the semi-Lagrangian model, the code is accurate enough to exhibit locally such trapping structures without any smoothing technique. Furthermore the size of such magnetic vortices depends on their location in the p_y momentum space, thus any type of average on p_y can smooth the information. For that reason we have adopted here to just observe, in a first step, the occurring of the magnetic trapping structures in global Vlasov- Maxwell simulations.

Owing to the very good resolution in phase space afforded by the semi-Lagrangian scheme, one can begin to understand the wave-particle interaction in greater details. Again dynamics of the selected particle stream is driven by the self-reorganisation of the magnetic field component B_z in term of magnetic trapping. This process is clearly visible in Fig. 18. We see that rotating filaments get thinner due to several rotations of the central trapping structure. Furthermore the distribution exhibits also a weak modulation on the mode $2k_0$ as a result of the presence of the Lorentz force. At time $t\omega_p = 60$, one sees the beginning of the formation of the magnetic trapping structure, which remains till the end of the simulation, strengthening the conjecture of a quasi-stationary solution in

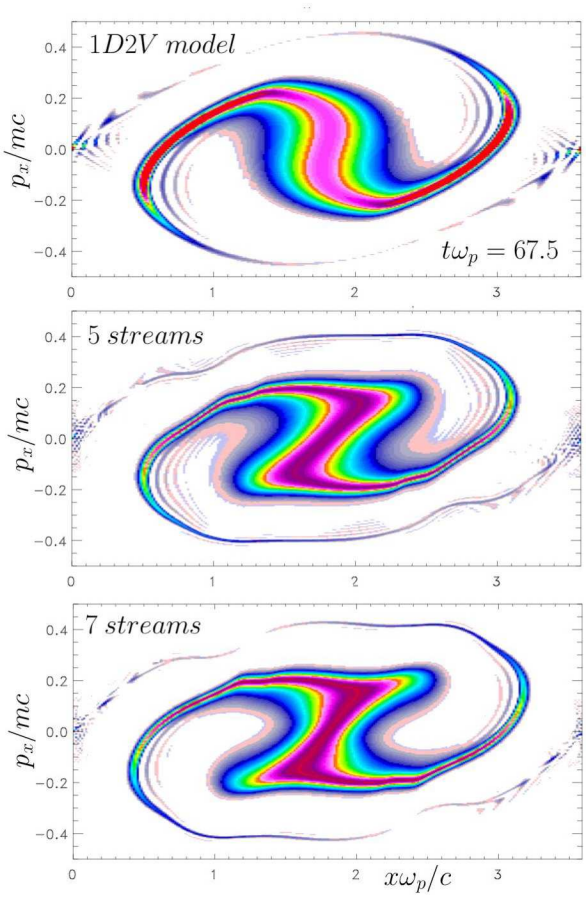

Figure 17: $x - p_x$ phase space representation of the particle stream located at the momentum value of $p_y = 2ma_y$ (a_y being the thermal velocity in p_y corresponding to a temperature of $T_y = 50keV$) and obtained from different models: on top panel the full kinetic 1D2V Vlasov-Maxwell solver, on middle panel, a view of the same particle stream from the multi-stream model with five streams, while on bottom panel, the last case with seven streams. In both simulations, the formation of the rotating magnetic structure, with thin "arms" are recovered. However note that the global form is somewhat different in the multi-stream approach.

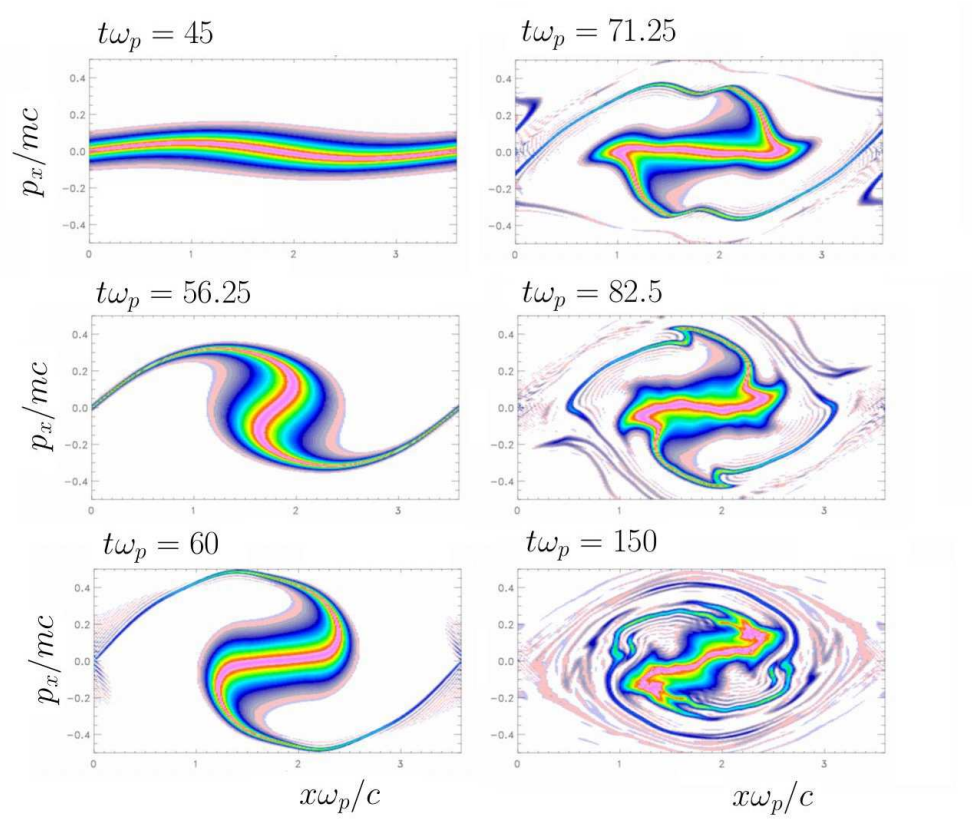

Figure 18: $x - p_x$ phase space representation of the particle stream, of very low density, initially located at $p_y = C_3 = 3ma_y$,at different times during the evolution. After several rotations, a weak modulation on the mode $2k_0$ is also occurring linked to the growth of the Lorentz force. Note also the occurring of a phase space mixing, at time $t\omega_p = 150$, due to the rotation of "arms". This simulation has been carried out with the multi-stream model with seven streams.

the asymptotic limit.

Our investigation reveals that it is the magnetic trapping which is here the dominant mechanism of saturation, although the longitudinal electric field energy is not null but nevertheless remains at a very low level. It is the perpendicular component of the kinetic energy (located in particle "streams") which is transferred to the magnetic field and into the longitudinal direction in momentum (giving rise to a longitudinal plasma heating). Thus the distribution function with the initial temperature anisotropy becomes unstable to WI whose consequence is to reduce the initial anisotropy. Fig.19 shows the two quantities $T_\perp$ (on top panel) and $T_\parallel$ (on bottom panel) determined as follows:

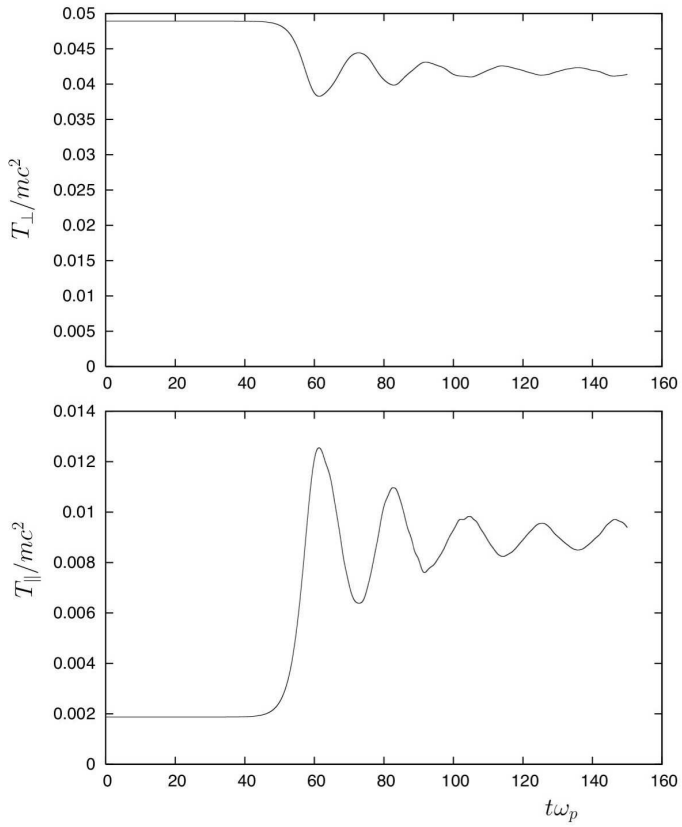

Figure 19: On top panel, the evolution of $k_B T_\perp/mc^2$ versus time while the normalized parallel temperature $k_B T_\parallel/mc^2$ is plotted on bottom panel (k_B was omitted in the notation). We observe clearly that $T_\parallel$ follows the time evolution of the magnetic energy $\epsilon_{m,z}$, plotted in Fig. 16. Results were obtained from the multi-stream model with five streams.

$$\frac{T_\perp}{mc^2} = \sum_{j=-N}^{+N} \frac{C_j^2}{m^2c^2} \iint \frac{f_j}{\gamma_j} dp_x dp_y \quad \text{and} \quad \frac{T_\parallel}{mc^2} = \sum_{j=-N}^{+N} \iint \frac{p_x^2}{m^2c^2} \frac{f_j}{\gamma_j} dp_x dp_y \qquad (58)$$

Results shown in Fig. 19 have been obtained from a simulation performed by the multi-stream code with five streams. We observe that $T_\parallel$ follows the temporal evolution of the

magnetic energy shown in Fig. 16. A closer look at the dynamics of "streams" reveals an even richer, but also more puzzling picture. The first striking feature is the occurring of a de-phasing between the streams j and $-j$ of type $f_{-j}(x,p_x,t) = f_j\left(x+\frac{L_x}{2},p_x,t\right)$ a feature observed in all simulations, even in the 2D full kinetic model. This implies that the quantity $\rho_j(x,t)$ defined in Eq. (27) verifies also the condition $\rho_{-j}(x,t) = \rho_j\left(x+\frac{L_x}{2},t\right)$. It turns out that the total current J_y can be written in the following form, by separating the different contributions of j:

$$J_y(x,t) = \sum_{j=-N}^{-1} J_{y,j}(x,t) + J_{y,0}(x,t) + \sum_{j=1}^{+N} J_{y,j}(x,t)$$

$$= \sum_{j=1}^{N} \frac{e}{m}\left(-C_j - eA_y(x,t)\right)\rho_{-j}(x,t) + J_{y,0}(x,t) + \sum_{j=1}^{+N} \frac{e}{m}\left(C_j - eA_y(x,t)\right)\rho_j(x,t) \quad (59)$$

If one assumes that $C_{-j} = -C_j$; $eA_y \ll C_j$ and that $J_{y,0}$ tends to zero, we see clearly that, it is this breaking in symmetry of type $f_{-j}(x,p_x,t) = f_j\left(x+\frac{L_x}{2},p_x,t\right)$ that allows the generation of a non zero current density between the components $J_{y,j}$ and $J_{y,-j}$. Indeed a symmetry of type $\rho_{-j}(x,t) = \rho_j(x,t)$ might lead to a zero contribution when A_y is negligible, i.e. at the beginning of the simulation, forbidding the start-up of the instability because the initial seed is not present. In addition since particles of the central stream experience a quasi-zero magnetic trapping (because $C_0 = 0$), we expect that the dominant mode is the one driven by the Lorentz force which leads then to the excitation of the electrostatic field and to the modulation on the mode $2k_0$.

By developing the term $\left(C_j - eA_y\right)^2$ we find, without difficulty, that the dominant term is $-2eA_y(x,t)\,C_j$ for all stream C_j with $C_j \neq 0$, while for the central stream, assuming that $C_0 = 0$, it is the Lorentz force $\sim e^2\partial_x\left(A_y^2\right)$ that becomes dominant, leading to the growth of the mode $2k_0$ by non linear effects. This situation is naturally encountered in regions of the bulk of the distribution in full kinetic simulations or in the central stream dynamics for the multi-stream model. Although the E_x field is much weaker in intensity when compared with the B_z component, its presence might nevertheless be very important, since it could accelerate particle to high energy through the growth of a plasma wave or drive secondary instabilities, a mechanism important in the relativistic regime.

Fig. 20 shows the advection motion of fast electrons in phase space, associated with the formation of thin filaments. The simulation was carried out with the 1D2V Vlasov solver. The initial "stream" population was chosen at $p_y = 0.50ma_y$, an intermediate position, a chosen value for which this set of parameter corresponds to the coupling between the two physical mechanisms present in the system: the vortex rotation induced by the magnetostatic field B_z (the E_y contribution usually has disappeared at that time)

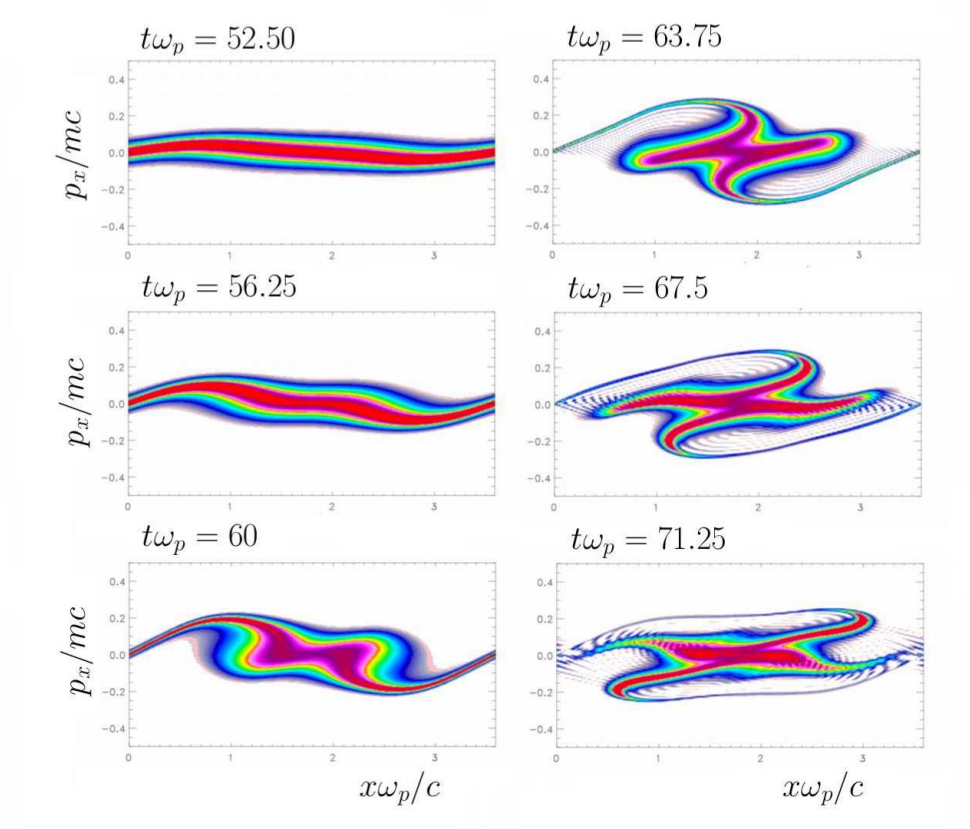

Figure 20: Phase space representation of a given particle population "bunch", initially located at the momentum value of $p_y = 0.5ma_y$, an intermediate position, for which the coupling with the Lorentz force takes place and leads to the advection motion of fast particles. Results presented here have been obtained from the 1D2V version of the Vlasov code.

and the weak acceleration of electrons driven by the electrostatic component E_x.

In the case of the multi-stream model, we have recovered that a small fraction of the magnetic energy is also converted in the electrostatic field. The diagnostics in phase space shows, as evidenced in Fig. 21, that particles of the central stream (with $C_0 = 0$) are accelerated in region of the X-point where the magnetic field B_z (or equivalently A_y) tends to zero. Due to the combined action of the Lorentz force, the resulting coupling between the electric potential on mode $2k_0$ and the magnetic trapping on mode k_0 seems to be the dominant process at saturation in the bulk of the plasma.

It is clear in Fig. 2 that the magnetic energy is the dominant part in comparison with the longitudinal electric part. What shows the multi-stream model is that the "particle stream" of the high canonical momentum experiences a strong magnetic trapping in comparison to the "central" stream. However for larger systems or if the dominant mode differs from k_0, a reorganisation of the plasma can be observed, even in presence of a weak electrostatic activity. Thus it has been observed by Ghizzo (2013c), that a self-reorganisation of the plasma begins at saturation with a symmetry-breaking instability of pair-wise merging of phase space vortices, where the plasma adjusts itself in wave number to give a stable state dominated now by trapping of mixed magnetic and electrostatic nature.

5 CONCLUSION

The multi-stream model appears to be an interesting alternative to the usual Vlasov kinetic description of the Weibel instability, driven by a temperature anisotropy. After recovering the key mechanisms in the saturation regime of WI and making the connection with the dynamics of "isolated" streams, it is a natural question to ask whether the features of WI can be recovered by using a small number of streams. The results of our investigation, based on both analytic treatment and numerical experiments, reveal that not only three streams are sufficient to reproduce the linear growth rate of WI, but also that a new physical insight may be allowed in the non linear regime by the model with at least five streams.

What emerges from the theoretical analysis and also from numerical investigations is the direct action on particle dynamics, of interaction between streams. An interesting consequence is the presence of a symmetry- breaking leading to a de-phasing of the fields allowing to explain the well-known Y-shape form of the plasma distribution in p_y and leading to the start-up of the instability.

One of the major merits of reduced models such as the multi-stream model or the fluid description with inclusion of the full pressure tensor dynamics is to provide a comprehensive understanding of the magnetic field generation and its feedback mechanism on

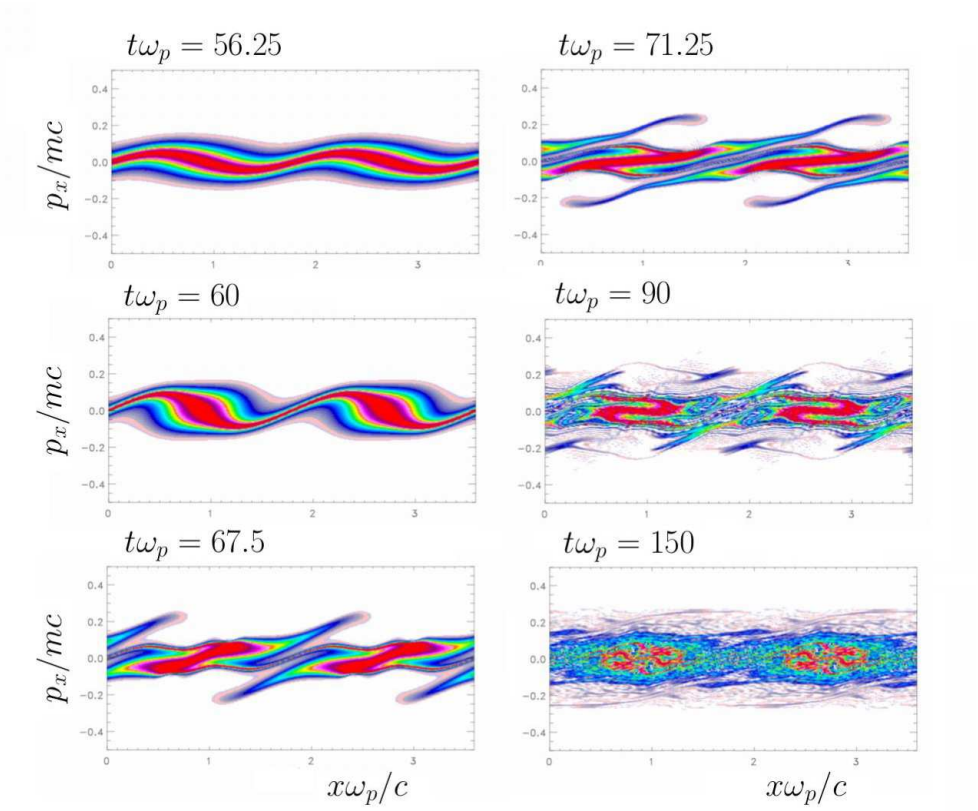

Figure 21: Behaviour of the central stream with $C_0 = 0$ in the $x - p_x$ phase space from the multi-stream model with five streams. We observe the importance of the mode $2k_0$ as already shown in Fig. 20 in the case of the full -kinetic 1D2V Vlasov code.

the electrostatic field generation, usually implicated into the self- reorganisation of the magnetic field in term of inverse-cascade (magnetic vortex coalescence) already observed in PIC or Vlasov simulation.

The philosophy used in the multi-stream model is reminiscent of the reduction procedure met in Hamiltonian theory or in particular of the multiple Water Bag model in which the choice of special conditions allows us to reduce the full kinetic Vlasov equation into a set of hydrodynamical equations. Certainly, the study of realistic problems for instance, would require more sophisticated models. In particular, one would want to investigate three-dimensional geometries, endowed with more complicated topological properties (without translation invariance for instance). In that case the multi-stream model must be ruled out, since it would imply the translation invariance

Though this will be the object of further work, we remark that these first results may provide an interesting basis for a quantitative comparison between both kinds of reduced models - the multi-stream model and the fluid description including the pressure tensor dynamics - still missing despite these two models are largely regarded as complementary in the physical description of collisionless plasmas due to the respective kinetic and fluid nature.

Acknowledgment

The authors are indebted to the IDRIS computational center, Orsay, France, for computer time allocation on their computers. This work was granted access to the HPC resources (Grant 2016- 057290) made by GENCI (Grand Equipement National de Calcul Intensif).

References

BASU B., 2002 Moment equation description of Weibel instability, Phys. Plasmas **9**, 5131 - 5134.

BEGUE M.L., GHIZZO A., BERTRAND P. 1999 Two-dimensional Vlasov simulation of Raman Scattering and Plasma Beatwave Acceleration on parallel computers, J. Comput. Phys **151**, 458- 478.

BRET A. 2009 Weibel Two-stream Filamentation, oblique, Bell, Buneman ... Which one grows faster?, The Astrophy. Journal **699**, 990- 1003.

BRET A. 2010 Exact relativistic kinetic theory of the full unstable spectrum of an electron-beam-plasma system with Maxwell-Juttner distribution functions, Phys. Rev. E, **81**, 036402.

BRET A., DEUTSCH C. 2006 A fluid approach to linear beam plasma electromagnetic instabilities, Phys. Plasmas, **13**, 042106- 01- 12..

BRET A., GREMILLET L., DIECKMAN M.E. 2010 Multidimensional electron beam-plasma instabilities in the relativistic regime, Phys. Plasmas **17**, 120501.

CERRUTI B., WERNER G.B., UZDENSKY D.A., BEGELMAN M.C. 2014 Gamma-ray flares in the Crab Nebula: A case of relativistic reconnection, Phys. Plasmas **21**, 056501.

DEL SARTO D., PEGORARO F., TENERANI A. 2015 Magneto-elastic waves in an anisotropic magnetised plasma, arXiv:1509.04938.

DEL SARTO D., PEGORARO F., CALIFANO F. 2016 Pressure anisotropy ans small spatial scales induced by velocity shear, Phys. Rev. E **93**, 053203.

FRIED B.D. 1959 Mechanism for instability of transverse plasma waves, Phys. Fluids, **2**, 337.

GHIZZO A., HUOT. F., BERTRAND P. 2003 A non periodic 2D semi-Lagrangian Vlasov code for laser-plasma interaction on parallel computer, J. Comput. Phys. **186**, 47-69.

GHIZZO A., BERTRAND P. 2013 On the multi-stream approach of relativistic Weibel instability. I Linear analysis and specific illustrations Phys. Plasmas **20**, 082109.

GHIZZO A. 2013 On the multi-stream approach of relativistic Weibel instability. II Bernstein- Greene- Kruskal type wave in magnetic trapping, Phys. Plasmas **20**, 082110.

GHIZZO A. 2013 On the multi-stream approach of relativistic Weibel instability. III. Comparison with full-kinetic Vlasov simulations, Phys. Plasmas **20**, 082111.

GHIZZO A., SARRAT M., DEL SARTO D. , SERRAT L. 2017 Parallel implementation of relativistic Semi-Lagrangian Vlasov-Maxwell solver, to be submitted to J. Comput. Phys.

INGLEBERT A., GHIZZO A., REVEILLE T., BERTRAND P., CALIFANO F. 2012 Multi-stream Vlasov model for the study of relativistic Weibel-type instabilities, Plasma Phys. Control. Fusion **54**, 085004.

INGLEBERT A., GHIZZO A., REVEILLE T., DEL SARTO D., BERTRAND P., CALIFANO F. 2011 A multi-stream Vlasov modeling unifying relativistic Weibel-type instabilities, Euro. Phys. Letters **95**, 45002

INNOCENTI M.E., LAZAR M., MARKIDIS S., LAPENTA G., POEDTS S. 2011 Electron streams formation and secondary two-stream instability onset in the post-saturation regime of the classical Weibel instability, Phys. Plasmas **18**, 052104-1-9.

KAANG H.H., RYV C.M., YOON P.H. 2009 Nonlinear saturation of relativistic Weibel instability driven by thermal anisotropy, Phys. Plasmas **16**, 082103.

LAZAR M., SCHLICKEISER R., WIELEBINSKI R., POEDTS S., 2009 Cosmological effects of Weibel-type instabilities, The Astro. Journal **693**, 1133- 1141.

LEMONS D.S, WINSKE D., GARY S.P. 1979 Nonlinear theory of the Weibel instability, J. Plasma Phys. **2**, 287-300.

MEDVEDEV M.V., SILVA L.O., KAMIONKOWSKI M. 2006 Cluster magnetic fields from large-scale structure and Galaxy cluster shocks, The Astro. Journal **642**, L1-4.

PALODHI L., CALIFANO F., PEGORARO F. 2010 On the transition between the Weibel and whistler instabilities, Plasm. Phys. Control. Fusion **52**, 095007- 1-13.

PALODHI L., CALIFANO F., PEGORARO F. 2009 Nonlinear kinetic development of the Weibel instability and the generation of electrostatic coherent structures, Plasma Phys. Control. Fus. **51**, 125006- 1-13

SARRAT M., DEL SARTO D., GHIZZO A. 2016 Fluid description of Weibel-type instabilities via full pressure tensor dynamics, Euro. Phys. Lett. **115**, 45001.

SARRAT M., DEL SARTO D., GHIZZO A. 2016 A pressure tensor description for time-resonant Weibel instability, to be submitted to J. Plas. Phys.

SCHLICKEISER R., SHUKLA P.K. 2003 Cosmological magnetic field generation by the Weibel instability, The Astro. Journal **599**, L57-60.

SCHOEFFLLER K.H., LOUREIRO N.F., FONSECA R.A., SILVA L.O. 2016 The generation of magnetic fields by the Biermann battery and the interplay with the Weibel instability, Phys. Plasmas **23**, 056304.

SHVETS G., POLOMAROV O., KHUDIK V., SIEMON C., KAGANOVICH I., 2009 Nonlinear evolution of the Weibel instability of relativistic electron beams, Phys. Plasmas **16**, 056303.

SILVA L.O., FONSECA R.A., TONGE J.W., MORI W.B., DAWSON J.M. 2002 On the role of the purely transverse Weibel instability in fast ignitor scenarios, Phys. Plasmas **9**, 2458.

WEIBEL E.S. 1959 Spontaneously growing transverse waves in a plasma due to an anisotropic velocity distribution, Phys. Rev. Lett. **2**, 83.